The Astrophysical Journal, 892:15 (16pp), 2020 March 20 https://doi.org/10.3847/1538-4357/ab7996

ASASSN-16oh: A Nova Outburst with No Mass Ejection—A New Type of Supersoft X-Ray Source in Old Populations

Mariko Kato[1], Hideyuki Saio[2], and Izumi Hachisu[3]
[1] Department of Astronomy, Keio University, Hiyoshi, Yokohama 223-8521, Japan; mariko.kato@hc.st.keio.ac.jp
[2] Astronomical Institute, Graduate School of Science, Tohoku University, Sendai 980-8578, Japan
[3] Department of Earth Science and Astronomy, College of Arts and Sciences, University of Tokyo, 3-8-1 Komaba, Meguro-ku, Tokyo 153-8902, Japan
Received 2019 November 1; revised 2020 February 17; accepted 2020 February 23; published 2020 March 23

Abstract

ASASSN-16oh is a peculiar transient supersoft X-ray source without a mass-ejection signature in the field of the Small Magellanic Cloud. Maccarone et al. concluded that ASASSN-16oh is the first dwarf nova with supersoft X-ray that originated from an equatorial accretion belt on a white dwarf (WD). Hillman et al. proposed a thermonuclear runaway model that both the X-rays and V/I photons are emitted from the hot WD. We propose a nova model induced by a high rate of mass accretion during a dwarf nova outburst, i.e., the X-rays originate from the surface of the hydrogen-burning WD whereas the V/I photons are from the irradiated disk. Our model explains the main observational properties of ASASSN-16oh. We also obtained thermonuclear runaway models with no mass ejection for a wide range of parameters of the WD mass and mass-accretion rates including both natural and forced novae in low-metal environments of $Z = 0.001$ and $Z = 0.0001$. They are a new type of periodic supersoft X-ray sources with no mass ejection and also a bright transient in V/I bands if they have a large disk. We suggest that such objects are candidates for Type Ia supernova progenitors because its mass is increasing at a very high efficiency (∼100%).

Unified Astronomy Thesaurus concepts: Novae (1127); Population II stars (1284); Dwarf novae (418)

1. Introduction

A nova is a thermonuclear runaway event on a mass-accreting white dwarf (WD). Novae usually brighten up by $\Delta V \sim 10$ mag or more in a few to tens of days and decline in a few months or years. After hydrogen ignites on the WD, the hydrogen-rich envelope expands to giant size and emits strong winds (e.g., Kato & Hachisu 1994). The nova brightness is dominated by free–free emission from optically thin ejecta outside the photosphere. Thus, the peak optical brightness depends on the maximum wind mass-loss rate (e.g., Hachisu & Kato 2006; Hachisu & Kato 2015). Due to strong mass loss, the envelope loses its mass, and the photosphere gradually shrinks and the photospheric temperature increases. Eventually, the nova enters a supersoft X-ray source (SSS) phase. The envelope mass decreases further due to nuclear burning after the winds stop. Hydrogen burning ends when the envelope mass reaches a critical value. By definition, a nova accompanies strong winds (mass ejection) in the optically bright phase.

On the other hand, a dwarf nova is an accretion event on a compact object, in which the mass accretion is enhanced by the thermal instability of the accretion disk. Dwarf novae usually brighten by $\Delta V \sim 2$–9 mag in a day or so and stays at that brightness from a few days to a few weeks. However, no SSS phase has ever been observed in dwarf nova outbursts.

ASASSN-16oh is a peculiar transient SSS in the field of the Small Magellanic Cloud (SMC), which was discovered by the All Sky Automated Survey for Supernovae (ASASSN) on UT 2016 December 2.15 (JD 2457,724.65) at $V = 16.9$ (Jha et al. 2016). The brightness reached an absolute magnitude of $M_V = -2.3$ on JD 2,457,744.6, where we assume that the distance modulus is $\mu_0 \equiv (m - M)_0 = 18.9$, and the absorption in the V band is $A_V = 0.13$ toward ASASSN-16oh (Jha et al. 2016; Mroz et al. 2016). The Optical Gravitational Lensing Experiment IV (OGLE IV) (Udalski et al. 2015) data show that the object was an irregular variable for several years with the quiescent luminosity of $I = 20.3$ and $V = 21.1$ (Maccarone et al. 2019).

The V and I light curves of ASASSN-16oh show a resemblance to those of long orbital-period dwarf novae such as V1017 Sgr in the peak brightness, outburst amplitude, and timescales (see Section 2 for details). The orbital period of V1017 Sgr is $P_{\rm orb} = 5.786$ days (Salazar et al. 2017). Therefore, Maccarone et al. (2019) expected the orbital period of ASASSN-16oh to be several days.

Maccarone et al. (2019) concluded that ASASSN-16oh is not a classical nova (thermonuclear runaway event) but an accretion event like a dwarf nova, mainly because of the (1) optical spectra showing a very narrow width of He II emission with no signature of mass ejection, (2) very slow rise (∼200 days) to the optical maximum compared with those of classical novae (a few days), and (3) rather dark peak V magnitude of $M_{V,\rm max} \sim -2.3$ compared with those of recurrent novae (e.g., the 1 yr recurrence period nova M31N 2008-12a of $M_{V,\rm max} = -7.2$; Darnley et al. 2015; Henze et al. 2018).

The only concern is the origin of supersoft X-rays because no SSS phase has been detected in dwarf nova outbursts. Maccarone et al. (2019) interpreted that supersoft X-rays could originate from a spreading layer around the equatorial accretion belt. This model requires a very high mass-accretion rate of $\sim 3 \times 10^{-7}\,M_\odot$ yr^{-1} (2×10^{19} g s^{-1}) on a very massive WD of $1.3\,M_\odot$ to support high temperatures and fluxes for supersoft X-ray.

The hot spreading layer of the accretion belt has not yet been studied in detail. If a disk around a massive WD with high accretion rates always accompanies a hot spreading layer, such supersoft X-rays could be observed in recurrent novae in their quiescent phase in U Sco ($M_{\rm WD} \sim 1.37\,M_\odot$ with $\dot{M}_{\rm acc} \sim 2.5 \times 10^{-7}\,M_\odot$ yr^{-1}, Hachisu et al. 2000) and RS Oph

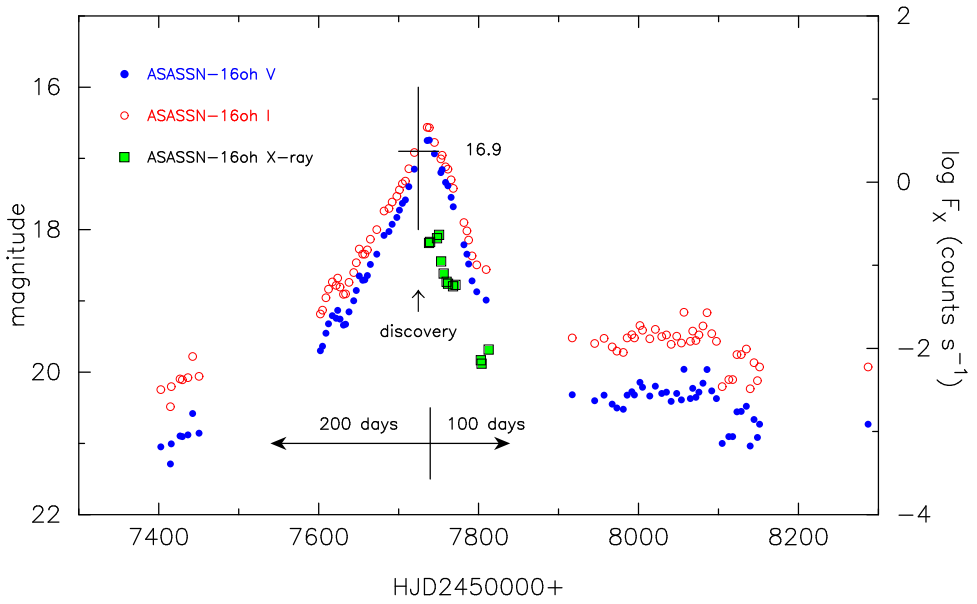

Figure 1. The I and V light curves of ASASSN-16oh as well as the soft X-ray count rates observed with *Swift*. The data are taken from the OGLE IV and *Swift* websites. The V magnitudes are estimated from the I data together with several $V-I$ colors in the outburst (see the main text for more details).

($\sim 1.35\,M_\odot$ with $\sim 2\times10^{-7}\,M_\odot$ yr^{-1}, Hachisu et al. 2008), but they have not yet been detected (see Section 6.4). This gives us the idea that the supersoft X-rays could originate from thermonuclear flashes on the WD.

It should be noted that the high instantaneous mass-accretion rate ($\sim 3\times10^{-7}\,M_\odot$ yr^{-1}; Maccarone et al. 2019) is close to the critical value to maintain steady hydrogen-shell burning, otherwise, there will only be very weak shell flashes (see, e.g., Figure 6 of Kato et al. 2014). With such a high rate of mass accretion, nova outbursts are so weak that wind mass loss is also weak. Moreover, a low-metallicity (low-Z) environment in the SMC suggests weak mass ejection during nova outbursts. These conditions led us to search for nova (thermonuclear runaway event) solutions for no mass ejection (e.g., Kato 1985; Kato & Hachisu 2009). They are periodically variable SSSs (e.g., Hachisu et al. 2016). Such an object has not been observationally detected yet.

Hillman et al. (2019) proposed another interpretation of ASASSN-16oh, a thermonuclear runaway event, and calculated several shell-flash models. They claimed that X-rays and V/I photons are emitted from a WD that undergoes hydrogen burning. However, it is unlikely that a hot WD with a surface temperature $T > 400{,}000$ K emits many low-energy V/I photons as well as X-rays. This concern led us to start the present work. We have calculated a nova model with the same parameters as Hillman et al.'s model and obtained different results. This will be presented in Section 5.

It is reasonable that X-rays and optical V/I photons come from different places in the binary system as noted by Maccarone et al. (2019). We regard the V/I photons to originate from a large accretion disk irradiated by the hot WD. We propose a recurrent nova (thermonuclear runaway) model for the supersoft X-rays and search the parameter region for no-mass-ejection novae. The main differences from Hillman et al. 's model are as follows: (1) the V/I photons originate from the accretion disk and companion star because the WD is too hot to emit many V/I photons. (2) To explain the observed X-ray light curve, the WD mass is much higher ($1.32\,M_\odot$) than that of Hillman et al.'s model ($1.1\,M_\odot$). (3) We suggest that the hydrogen-shell flash could be triggered by a massive mass inflow during a dwarf nova outburst.

Both models of dwarf nova (Maccarone et al. 2019) and thermonuclear shell flash (present work) are based on the presence of a mass-accreting massive WD ($M_{\rm WD} \gtrsim 1.3\,M_\odot$) in ASASSN-16oh. In the latter model, the WD mass increases steadily because there is no mass ejection during the flash. Such a massive mass-increasing WD in a low-Z environment is very interesting in binary evolution scenarios because it could be a new kind of candidate for Type Ia supernova (SN Ia) progenitors.

The aim of this work is to present a theoretical model of ASASSN-16oh as well as to search for a possible region of novae with no mass ejection in low-metallicity environments. We organize the present paper as follows. First, we summarize the observational properties of ASASSN-16oh in Section 2. Then, we briefly introduce the possible parameter region for nova outbursts without mass ejection, including both forced and natural novae in Section 3. Our results are presented in Sections 4. We examine Hillman et al.'s (2019) nova model in Section 5, and compare our model with Maccarone et al.'s model in Section 6. Discussion and conclusions follow in Sections 7 and 8, respectively.

2. Observational Properties of ASASSN-16oh

In this section, we summarize the characteristic properties of ASASSN-16oh.

2.1. V/I Light Curves

We plot the I magnitudes of ASASSN-16oh in Figure 1 (unfilled red circles), taken from the OGLE IV website (Mroz et al. 2016; Maccarone et al. 2019).

For later use, we have estimated the V light curve from the I data and several $V-I$ colors listed in Maccarone et al. (2019): $V-I=0.8$ in quiescent phase, $V-I=0.36$ on JD 2457657.7, $V-I=0.34$ on JD 2457681.78, and $V-I=0.16$ on JD 2457744.6. With a linear interpolation of these $V-I$ data and assumed (start, end) of the outburst to

be (200 days before, 100 days after) the I peak (JD 2457737.1), we recover the V magnitudes (filled blue circles) as shown in Figure 1. We assumed that the I brightness reaches a maximum on JD 2457737.1 from an interpolation of the other I data.

The characteristic property of the light curve is a slow rise, sharp peak followed by rapid decay. The brightness rises slowly in ~200 days and declines fast in ~100 days. These properties are unlike those of typical nova outbursts but rather similar to long orbital-period dwarf novae. For example, the dwarf nova outbursts of V1017 Sgr show a 90 day rise and 90 day decline with an almost symmetric light-curve shape. In contrast, a typical nova rises within a few days and decays much slowly over a timescale of years (see, e.g., Figure 1 of Hachisu & Kato 2015).

There are other common properties between ASASSN-16oh and the dwarf nova V1017 Sgr. The peak V brightness is $M_{V,\max} \sim -2.3$ in ASASSN-16oh, similar to $M_{V,\max} \sim -1.3$ in V1017 Sgr (Schaefer 2018). The quiescent brightnesses of both objects are also similar, that is, $M_{V,\min} \approx 2.1$ for ASASSN-16oh and $M_{V,\min} \approx 1.8$ for V1017 Sgr (Schaefer 2018). Thus, the light-curve shape of ASASSN-16oh may be explained as a long orbital-period dwarf nova.

2.2. Optical Spectrum

Maccarone et al. (2019) presented the Southern African Large Telescope optical spectrum of ASASSN-16oh taken on UT 2016 December 16–24 (JD 2457738.5–245746.5), just after the I peak (JD 2457737.1). This spectrum shows no indication of mass loss, such as many broad emission lines or P-Cygni profiles usually seen in classical novae. Thus, if this is a classical nova phenomenon, it is a rare case in which no wind mass-loss occurs.

2.3. X-Ray Light Curve and Spectrum

A distinct difference between ASASSN-16oh and dwarf novae is the supersoft X-ray detection. No SSS phase has ever been detected in dwarf novae while an SSS phase is frequently observed in classical novae (Schwarz et al. 2011). If ASASSN-16oh is a dwarf nova, this is the first case of supersoft X-ray detection (Maccarone et al. 2019).

Figure 1 also shows the X-ray count rates observed with *Swift* (0.3–10.0 keV: filled green squares outlined with a black line). It seems that the X-ray count rate reaches maximum slightly later than the I peak and decays with the I light curve.

The X-ray spectra are dominated by soft components. Maccarone et al. (2019) deduced a blackbody temperature of 900,000 K and a flux of $\sim 1 \times 10^{37}$ erg s^{-1} from the *Swift*/XRT spectrum on UT 2016 December 15 (JD 2,457,737.5) at the distance of the SMC. From the *Chandra*/LETG spectrum taken on UT 2016 December 28 (JD 2,457,750.5), Maccarone et al. (2019) derived a blackbody temperature of 905,000 K, a luminosity of 6.7×10^{36} erg s^{-1}, and the hydrogen column density of $N_{\rm H} = 3.4 \times 10^{20}$ cm^{-2}, and, for an atmosphere model of solar abundance, 750,000 K and $N_{\rm H} = 2.0 \times 10^{20}$ cm^{-2}. Hillman et al. (2019) reanalyzed the same *Chandra* spectrum obtained by Maccarone et al. (2019) with a metal-poor atmosphere model and obtained the effective temperature of 750,000 K, the bolometric luminosity of 4.3×10^{36} erg s^{-1}, and the hydrogen column density of $N_{\rm H} = 2.3 \times 10^{20}$ cm^{-2}.

These temperatures are consistent with the surface temperatures of massive WDs in the SSS phase of classical novae (e.g., Kato 1997; Schwarz et al. 2011). Thus, a nuclear-burning origin seems to be a natural explanation for the X-rays.

2.4. Column Density and Unabsorbed X-Ray Flux

Both Maccarone et al. (2019) and Hillman et al. (2019) obtained a similar column density of $N_{\rm H} = 2 \times 10^{20}$ cm^{-2} that can be converted to $E(B-V) = N_{\rm H}/5.8 \times 10^{21} \approx 0.035$ (Bohlin et al. 1978), $E(B-V) = N_{\rm H}/6.8 \times 10^{21} \approx 0.03$ (Güver & Özel 2009), or $E(B-V) = N_{\rm H}/8.3 \times 10^{21} \approx 0.024$ (Liszt 2014). In the present paper, we adopt $A_V = 3.1E(B-V) = 0.1$, $(m-M)_V = 18.9 + 0.1 = 19.0$, and $(m-M)_I = 18.95$.

Maccarone et al. (2019) obtained the unabsorbed X-ray luminosity to be $\sim 1 \times 10^{37}$ erg s^{-1} from the *Swift*/XRT spectrum and to be 6.7×10^{36} erg s^{-1} from the *Chandra*/LETG spectrum. Hillman et al. (2019) obtained the unabsorbed X-ray flux to be 4.3×10^{36} erg s^{-1}.

These luminosities are much lower than the Eddington luminosity $\sim 1 \times 10^{38}$ erg s^{-1} for a $1.0\,M_\odot$ WD. If it is a classical nova outburst, the X-ray luminosity from the naked WD is close to the Eddington limit. Hillman et al. (2019) suggested that the low brightness is owing to occultation by the accretion disk rim as in the recurrent nova U Sco, although they did not include effects of the accretion disk in their V light-curve model. Orio et al. (2013) estimated the unabsorbed X-ray luminosity of U Sco in the SSS phase to be $\sim 7 \times 10^{36}$ erg s^{-1} from the *Chandra*/HRC-S and LETG spectra. The surface of the WD is occulted by the disk rim and the X-rays come from Thomson scattering by expanded plasma around the WD. This X-ray luminosity is similar to that of ASASSN-16oh.

2.5. V − I *Color: Evidence 1 for an Irradiated Accretion Disk*

Figure 2 shows the color–magnitude diagram, $(V-I)_0$–M_I, of ASASSN-16oh around the peak of the outburst ($t = -79.4$, -55.3, and $+7.5$ days after the I peak). Here, $(V-I)_0$ is the intrinsic $V-I$ color, which is calculated from the relation $(V-I)_0 = (V-I) - 1.6E(B-V)$ (Rieke & Lebofsky 1985), and M_I is the absolute I magnitude.

Figure 2 also shows the color–magnitude track of the recurrent nova U Sco in the 2010 outburst. We assume the distance modulus in the I band to be $(m-M)_I = 15.9$ and the reddening to be $E(B-V) = 0.26$ after Hachisu & Kato (2018). The $UBVI_{\rm C}$ data of U Sco are taken from Pagnotta et al. (2015). Except for the short period after the peak ($M_I < -5$), the $(V-I)_0$ color of U Sco is almost constant, i.e., $(V-I)_0 \sim 0.1 - 0.2$. U Sco has an irradiated accretion disk with the radius of $\sim 2.5\,R_\odot$ (Hachisu et al. 2000). U Sco entered a plateau phase in the V/I light curves when $I > 14$, that is, when $M_I \gtrsim -5$ as shown in Figure 2 of Pagnotta et al. (2015). This is because the V and I brightnesses are dominated by the irradiated accretion disk (Hachisu et al. 2000). This plateau phase corresponds almost to the SSS phase. The $(V-I)_0$ colors of ASASSN-16oh well overlap those of U Sco in its SSS phase (when $M_I \gtrsim -2$).

For comparison, we further add the track of a typical classical nova, V496 Sct. We assume the distance modulus in the I band to be $(m-M)_I = 13.0$ and the reddening to be $E(B-V) = 0.45$ after Hachisu & Kato (2019a). The $BVI_{\rm C}$ data of V496 Sct are taken from the archives of the Variable Star Observers League of Japan, the American Association of Variable Star Observers, the Small and Medium Aperture

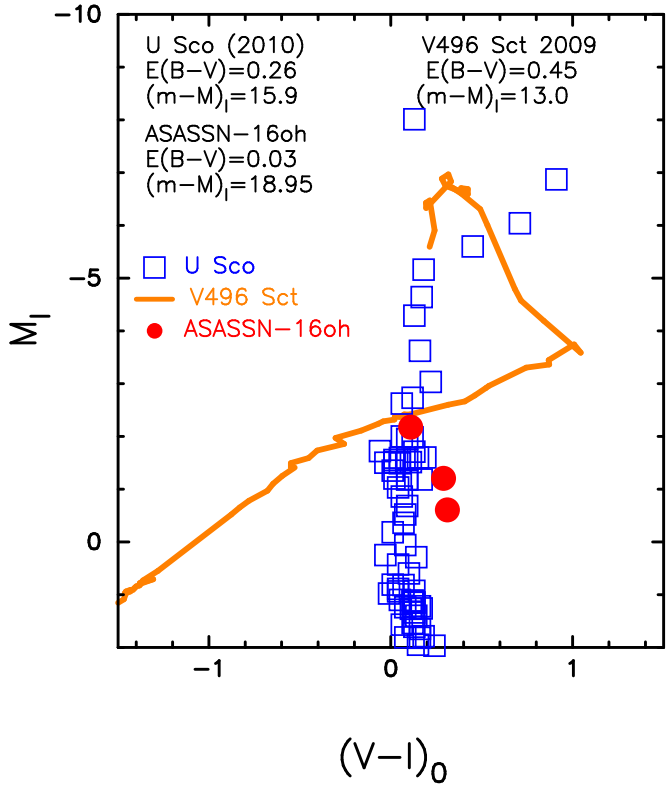

Figure 2. The $(V-I)_0$–M_I color–magnitude diagram of ASASSN-16oh (filled red circles) in outburst. Here, $(V-I)_0$ is the intrinsic $V-I$ color and M_I is the absolute I magnitude and $(V-I)_0$ is calculated from the relation of $(V-I)_0=(V-I)-1.6E(B-V)$ (Rieke & Lebofsky 1985). The three $V-I$ colors of ASASSN-16oh are $V-I=0.36$ (JD 2457657.7), $V-I=0.34$ (JD 2457681.78), and $V-I=0.16$ (JD 2457744.6). For comparison, the color–magnitude tracks of the recurrent nova U Sco (open blue square) and the classical nova V496 Sct (orange line) are added. The distance modulus and color excess of $(m-M)_I=15.9$ and $E(B-V)=0.26$ (U Sco), and 13.0 and 0.45 (V496 Sct) are taken from Hachisu & Kato (2018) and Hachisu & Kato (2019a), respectively.

Telescope System (Walter et al. 2012), and Raj et al. (2012). The V and I light curves are plotted in Figure 52 of Hachisu & Kato (2019a) and the $(V-I)_0$–M_I color–magnitude diagram is presented in Hachisu & Kato (2019b). In usual classical novae, their optical spectra are dominated by free–free emission from optically thin ejecta. After the optical peak, the optical brightness monotonically decreases with time and its color goes toward the red, due mainly to the emission line effect in the I band such as the O I and Ca II triplet. In the later phase ($M_I>-4$), the nova enters the nebular phase, and strong emission lines such as [O III] contribute to the V band. Then, the $V-I$ color turns to the blue. No X-ray data of V496 Sct are available, but the nova should enter the SSS phase when it declined to $M_I>0$ as shown in Figures 50 and 52 of Hachisu & Kato (2019a).

In general, classical novae are short orbital-period binaries of $P_{\rm orb}\sim$ a few hours. They have an accretion disk with the radius of $\sim 0.5\,R_\odot$, the brightness of which is rather faint in the SSS phase. Even if the accretion disk survives after the nova outburst, it is deeply embedded in the ejecta. In the nebular phase, the accretion disk appears because the ejecta becomes optically thin, but it is too small to contribute to the luminosity and color.

In contrast, U Sco has a large accretion disk with the radius of $\sim 2.5\,R_\odot$ because the orbital period is $P_{\rm orb}=1.23$ days and its binary size (separation) is $a\sim 6$–$7\,R_\odot$ (Hachisu et al. 2000). Therefore, the irradiated disk substantially contributes to the V and I bands in the SSS phase (Hachisu et al. 2000). This is partly because the ejecta mass of U Sco is very small, and the nebular emission line effect is relatively small. These physical properties give rise to the color-evolution difference between U Sco and V496 Sct.

Because the $(V-I)_0$ color in the SSS phase is similar between ASASSN-16oh and U Sco, we expect that the V and I brightnesses of ASASSN-16oh originate from the irradiated accretion disk, like U Sco.

2.6. M_V Light Curve: Evidence 2 for an Irradiated Accretion Disk

To further confirm the presence of an irradiated large accretion disk in ASASSN-16oh, we compare the absolute V magnitude with two other binaries that have a prominent irradiated accretion disk. One is the galactic recurrent nova U Sco and the other is the Large Magellanic Cloud (LMC) SSS RX J0513.9−6951.

2.6.1. U Sco

Figure 3(a) shows the light curve of U Sco in the 2010 outburst. We adopt the distance modulus in the V band to be $(m-M)_V=16.3$ (Hachisu & Kato 2018). Around the optical peak, the brightness is dominated by the emission from the ejecta. As time goes on, the ejecta becomes optically thin and the continuum emission from the irradiated disk becomes dominant. In the SSS phase, the light curve shows a plateau because its brightness is dominated by the irradiated accretion disk. The disk keeps a constant brightness until the nuclear burning turns off around JD 2445,260.

We add the absolute V magnitude, M_V, light curve of ASASSN-16oh to compare with that of U Sco. Here, the timescale of ASASSN-16oh is squeezed 5.5 times and the origin of time is shifted to match their supersoft X-ray peaks.

This figure demonstrates that the peak absolute magnitude M_V of ASASSN-16oh is roughly the same as that of U Sco in the SSS phase. We expect that a larger irradiated disk is brighter. Thus, a rough agreement of the absolute brightness indicates that the sizes of the accretion disks are comparable. The orbital period of U Sco is $P_{\rm orb}=1.23$ days (Schaefer & Ringwald 1995), and the disk size is $\sim 2.5\,R_\odot$ (Hachisu et al. 2000). This is broadly consistent with the orbital period (several days) of ASASSN-16oh suggested by Maccarone et al. (2019).

2.6.2. RX J0513.9−6951

We also compare ASASSN-16oh with RX J0513.9−6951. This object shows a periodic variation in the V magnitude as shown in Figure 3(b). Here we adopt the distance modulus in the V band of RX J0513.9−6951 to be $(m-M)_V=\mu_0+3.1\times E(B-V)$ $=18.5+3.1\times 0.12=18.9$. We have $\mu_0=18.5$ (Pietrzyński et al. 2011) and $E(B-V)=0.12$ (Imara & Blitz 2007) toward the LMC. The supersoft X-ray flux is observed in the optical low state.

Hachisu & Kato (2003) modeled this object with a binary consisting of an accreting WD, large accretion disk, and lobe-filling companion star. The mass-accretion rate $\dot{M}_{\rm acc}>10^{-6}\,M_\odot$ yr^{-1} is above the stability line so that

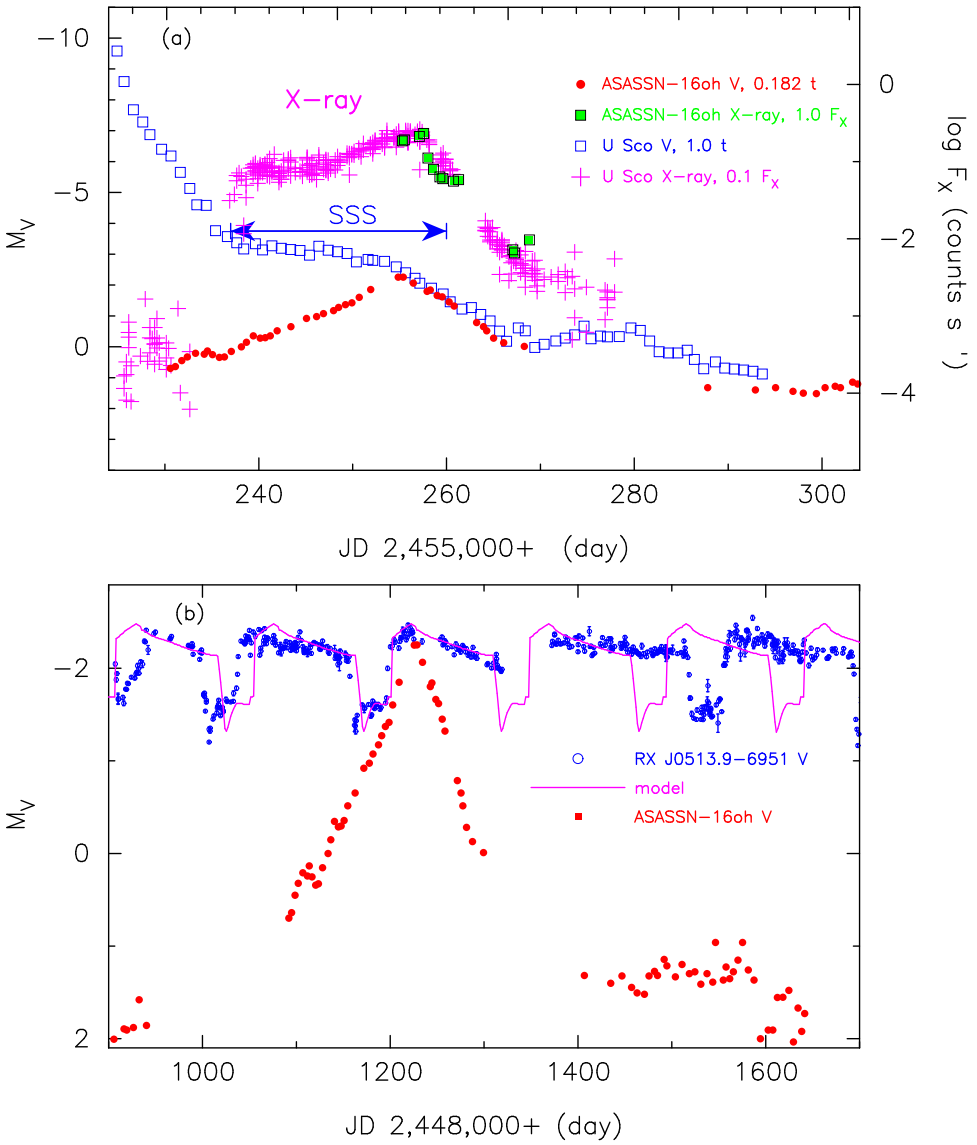

Figure 3. (a) The V and supersoft X-ray light curves of the recurrent nova U Sco (2010) compared with the V light curve of ASASSN-16oh. The data of U Sco are taken from Pagnotta et al. (2015). The X-ray data are taken from the *Swift* website (Evans et al. 2009). The timescale of ASASSN-16oh is squeezed 5.5 times. The peak brightness of ASASSN-16oh is compatible with the brightness of U Sco in the SSS phase. The V brightness of U Sco in the SSS phase can be explained by a large accretion disk irradiated by a central hot WD (see, e.g., Hachisu et al. 2000). (b) The V light curve of the LMC supersoft X-ray source RX J0513.9−6951 and a model light curve (solid magenta line) calculated by Hachisu & Kato (2003). The data of RX J0513.9−6951 are the same as those in Hachisu & Kato (2003). We add the V light curve of ASASSN-16oh for comparison, assuming $(m - M)_V = 19.0$.

hydrogen is stably burning. Thus, the WD is always as bright as the Eddington luminosity. At the beginning, the mass-transfer rate is larger than the critical rate of the wind ($\dot{M}_{\rm cr}$; see, e.g., Figure 6 of Kato et al. 2014). The WD envelope expands to emit strong winds. The winds hit the surface of the companion star and strip off the very surface layer. This effect works to reduce or stop the mass transfer. The WD envelope shrinks, and the winds stop. The temperature of the WD photosphere increases and the main emitting wavelength region moves to supersoft X-rays. The very surface layer of the companion star recovers its original radius in a thermal timescale, and the mass transfer restarts. The high-rate mass accretion onto the WD is further delayed by a viscous timescale of the accretion disk. After a total time of recovery (thermal timescale) and diffusion (viscous timescale), the high rate of mass accretion recovers. This is the mechanism of periodic variation of mass transfer.

In the wind phase, the surface of the accretion disk is blown in the wind and the optically thick region of the accretion disk is enlarged to beyond the size of the binary. Because the irradiated surface area becomes large, it brightens up. This is the optical high state. When the winds stop, the size of the accretion disk comes back to the original size. Its brightness declines. This is the optical low state in the V band. Thus, the optical high state corresponds to the wind phase and expanded accretion disk. In a model of Hachisu & Kato (2003), the optically thick region of the accretion disk expands comparably to the binary separation, $a = 5.53\,R_\odot$, for their binary model of $M_{\rm WD} = 1.3\,M_\odot$ and $M_2 = 2.6\,M_\odot$. The orbital period is $P_{\rm orb} = 0.76$ days (Pakull et al. 1993).

We add the ASASSN-16oh data to Figure 3(b) in the same timescale. The peak $M_{V,\rm max}$ of ASASSN-16oh is almost the same as the optical high state of RX J0513.9−6951. This is

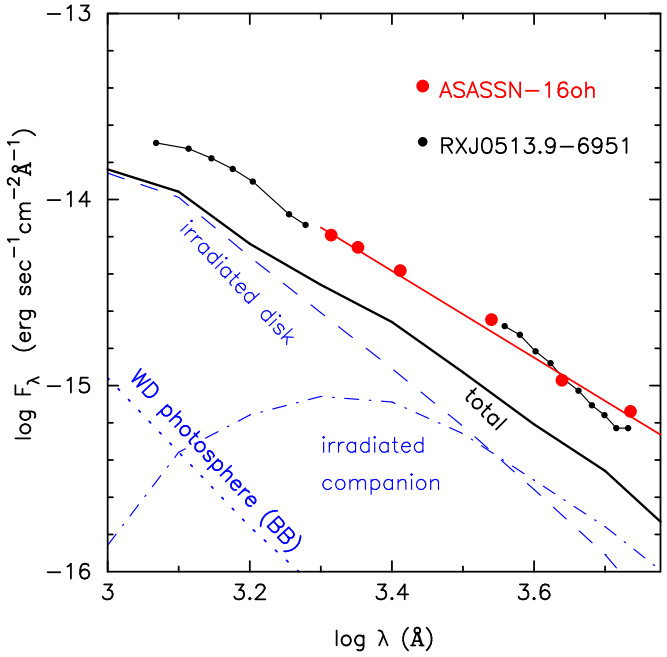

Figure 4. Spectral energy distribution of ASASSN-16oh (red dot: taken from Maccarone et al. 2019) compared with RX J0513.9−6951 (black dot connected with a solid line: Pakull et al. 1993). The red line indicates the inclination of the $F_\lambda \propto \lambda^{-2.33}$ law (Maccarone et al. 2019). The black and blue lines represent a theoretical model (taken from Popham & Di Stefano 1996) for a supersoft X-ray source that consists of a steady burning WD (labeled BB, dotted line), irradiated accretion disk (dashed line), and irradiated companion star (dashed −dotted line). The total flux (thick solid black line), which is the summation of these three, shows a similar spectrum energy distribution to ASASSN-16oh and RX J0513.9−6951. The theoretical lines and fluxes of RX J0513.9−6951 are shifted downward by $\log(60\ \mathrm{kpc}/50\ \mathrm{kpc})^2 = 0.158$ to compensate for the distance difference between the SMC and LMC.

also an indication that ASASSN-16oh has a large irradiated disk comparable to that in RX J0513.9−6951.

2.7. UV/Optical SED: Evidence 3 for an Irradiated Accretion Disk

Maccarone et al. (2019) obtained the spectral energy distribution (SED) of ASASSN-16oh from 2000 to 6000 Å that is well approximated by a power law of $F_\lambda \propto \lambda^{-2.33}$ as in Figure 4. Here, F_λ is the energy flux at the wavelength λ. For comparison, we added the continuum flux of the LMC SSS RX J0513.9−6951, which is taken from the spectrum observed with the *International Ultraviolet Explore* (*IUE*)/SWP and 2.2 m Max-Planck ESO telescope (Pakull et al. 1993). This spectrum shows a resemblance to ASASSN-16oh, suggesting that the binary is consistent with a nuclear-burning WD, irradiated accretion disk, and lobe-filling companion star like RX J0513.9−6951. We also add a model spectrum calculated by Popham & Di Stefano (1996) for LMC SSSs (thick solid black line). This model consists of a steady burning WD, irradiated accretion disk, and lobe-filling companion star. The total flux, which is the summation of these three components, well reproduces the $F_\lambda \propto \lambda^{-2.33}$ law. The irradiated accretion disk dominantly contributes to the total flux, whereas the irradiated secondary star contributes only to the optical region. The contribution from the WD photosphere is negligible. The agreement in the SED between RX J0513.9−6951 and ASASSN-16oh also suggests the presence of an irradiated accretion disk in ASASSN-16oh. We will discuss this point in more detail in Section 6.2.

3. Numerical Calculation of Hydrogen-shell Flashes with No Mass Ejection

Based on the observational properties of ASASSN-16oh, it is natural to assume that X-rays and optical V/I emission originate from different places in the binary. We regard the V/I band emission to come from an irradiated accretion disk and companion star, and the X-rays from a hot WD surface. Here, we focus our thoughts on shell-flash models that show no mass ejection.

3.1. Novae without Mass Ejection

By definition, novae accompany strong and fast mass ejection (or strong and fast wind mass loss; see, e.g., Warner 1995). The optically thick winds are accelerated when the photospheric luminosity approaches the Eddington luminosity. Because the OPAL opacity has a prominent peak at $\log T$ (K) ~ 5.2 owing to iron ionization (Iglesias & Rogers 1996), the optically thick winds are accelerated around this temperature region, i.e., deep inside the photosphere. The occurrence condition of winds was examined first by Kato (1985) for the old opacities and then by Kato & Hachisu (2009) and Kato et al. (2013) for the OPAL opacities (Iglesias & Rogers 1996). These works clarified that WDs do not emit optically thick winds in the following cases.

1. In low-mass WDs, the wind acceleration is insufficient such that the wind velocity at the photosphere does not exceed the escape velocity there. The envelope simply expands and then shrinks without mass ejection. This occurs in low-mass WDs of $M_{\rm WD} < 0.5$–$0.6\,M_\odot$ for the metallicity of $Z = 0.02$ (Kato & Hachisu 2009). The galactic slow nova PU Vul corresponds to this case (Kato et al. 2011, 2012).
2. When the mass-accretion rate is high and the ignition mass is very small, the envelope does not expand to reach $\log T$ (K) ~ 5.2 at the photosphere. Winds are not accelerated (Kato & Hachisu 2009).
3. In old population novae, the metallicity is very low so that the iron peak in the OPAL opacity is not high enough to accelerate winds (Kato et al. 2013).
4. When the mass-accretion rate is higher than the stability line of steady hydrogen burning $\dot{M}_{\rm acc} > \dot{M}_{\rm stable}$, we can make a forced nova with no mass ejection by manipulating the stop/restart of mass accretion. This will be explained in Section 3.3.

Among a huge number of galactic novae ($Z \sim 0.02$), only one (PU Vul) is known to be an object without optically thick winds. ASASSN-16oh is an SMC object and could be in a low-Z environment. With a lower Z, the wind acceleration is weaker because the lower iron abundance results in a smaller peak in the OPAL opacity. Kato et al. (2013) studied starts/ends of winds in various populations based on their steady-state approach. This approximation may not be good in the rising phase of strong nova outbursts. In this work, we study the occurrence of winds using a stellar evolution code (Kato et al. 2017b).

3.2. Method and Model Parameters

Our numerical code is the same as that described in Kato et al. (2017b). When the hydrogen-rich envelope of the WD expands after hydrogen ignites, wind mass loss often occurs. Henyey-type codes, widely used in stellar evolution calculation, have difficulties calculating extended stages of nova outbursts. This led many authors to assume some mass loss in their numerical codes to continue calculation, but these mass-loss rates are not based on reliable acceleration mechanism of nova winds (Kato et al. 2017a). Kato et al. (2017b) introduced how to obtain the mass-loss rate consistent with optically thick winds (Kato & Hachisu 1994). This method is to connect an interior structure with an outer wind solution and needs many iterations and human time until we obtain the final value of the mass-loss rate. In the present paper, we focus our calculation on no-mass-ejection novae. Therefore, without such an iteration process, we simply assume, if needed, a tentative mass-loss rate described by Equation (1) of Kato et al. (2017b).

We assume Population II composition for accreted matter, i.e., $X = 0.75$, $Y = 0.249$, and $Z = 0.001$, where X is hydrogen, Y is helium, and Z is the heavy element content in mass weight. This corresponds to a typical metallicity of the SMC ([Fe/H] $= -1.25 \pm 0.01$; Cioni 2009).

The WD mass and mass-accretion rate of our models are plotted in Figure 5, which is the diagram of WD response for various WD masses and mass-accretion rates. Below the stability line of steady hydrogen burning (lower black line labeled $\dot{M}_{\rm stable}$), hydrogen-shell burning is unstable and the accreting WDs experience periodic shell flashes, i.e., nova outbursts. The equi-recurrence period of shell flashes is depicted by the cyan-blue lines, with the period beside each line. The crosses represent no-mass-ejection models, while the open circles depict models in which we assume mass loss; otherwise, our calculation does not converge.

Above the stability line, the photospheric radius is larger for a larger mass-accretion rate. In the region to the left of the vertical blue line ($M_{\rm WD} \lesssim 1.15\,M_\odot$), the envelope eventually expands to giant size without mass loss. The optically thick wind mass loss occurs only in the region above the upper horizontal black line and to the right of the vertical blue line, i.e., very massive WDs ($M_{\rm WD} \gtrsim 1.15\,M_\odot$) and high mass-accretion rates ($\dot{M}_{\rm acc} \gtrsim 6 \times 10^{-7} M_\odot$ yr^{-1}).

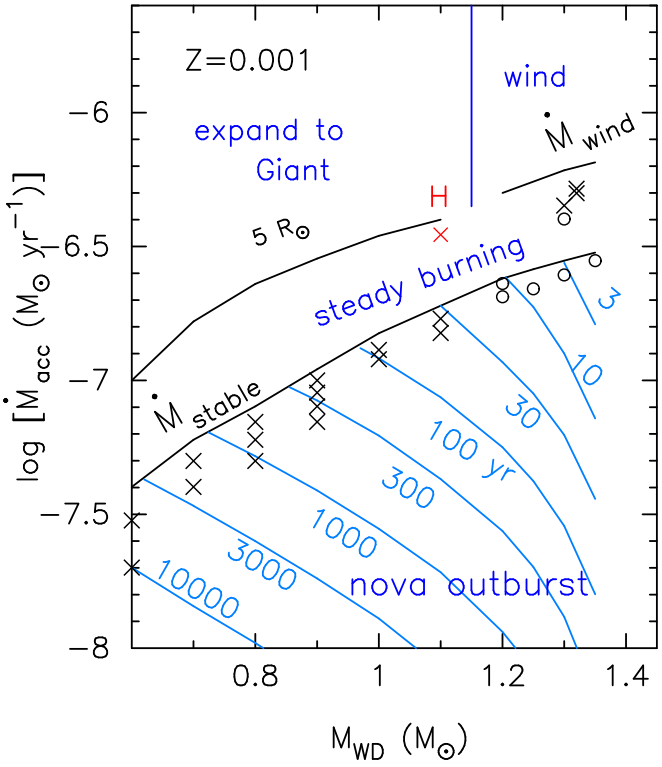

Figure 5. The responses of WDs in the mass-accretion rate vs. WD mass diagram. Below the stability line labeled $\dot{M}_{\rm stable}$, hydrogen-shell burning is thermally unstable and the WD experiences repeated shell flashes. Above the line, hydrogen burning is stable, and no repeated shell flashes occur unless the mass-accretion rate is manipulated by some mechanisms (forced novae). The crosses denote the models in which no mass ejection occurs during the outburst while the open circles correspond to the models with mass loss. The upper solid line labeled $5\,R_\odot$ shows the place at which the photospheric radius reaches $5\,R_\odot$. Above the line, the photosphere could be larger than the binary separation and a common envelope evolution may occur. In the region to the right of the vertical blue line, optically thick winds are accelerated and the binary may experience an accretion wind evolution, avoiding a common envelope evolution. The red cross labeled "H" is Hillman et al.'s (2019) model, which is above the stability line, and their model is intrinsically a forced nova (see Section 5).

3.3. Forced Novae and Natural Novae

Figure 6 shows the last four cycles of our three models. No mass ejection occurs in any of the models in this figure. The first two are close to but below the stability line, i.e., (a) $M_{\rm WD} = 1.0\,M_\odot$ with $\dot{M}_{\rm acc} = 1.2 \times 10^{-7} M_\odot$ yr^{-1} and (b) $M_{\rm WD} = 1.1\,M_\odot$ with $\dot{M}_{\rm acc} = 1.5 \times 10^{-7}\,M_\odot$ yr^{-1}. The WD always accretes matter. The accretion rate is smaller than the nuclear-burning rate during the flash ($\dot{M}_{\rm acc} < \dot{M}_{\rm nuc}$), then the envelope mass gradually decreases ($\dot{M}_{\rm env} = \dot{M}_{\rm acc} - \dot{M}_{\rm nuc} < 0$) to below the minimum envelope mass for hydrogen burning. Thus, hydrogen burning eventually ends. We call the novae that occur below the stability line "natural nova" to distinguish them from the "forced novae" that occur above the stability line (Hachisu et al. 2016).

Figure 6(c) shows an example of a forced nova, i.e., $M_{\rm WD} = 1.3\,M_\odot$ with $\dot{M}_{\rm acc} = 4.5 \times 10^{-7}\,M_\odot$ yr^{-1}, being located above the stability line. In this region, the nuclear-burning rate is balanced by the accretion rate ($\dot{M}_{\rm env} = \dot{M}_{\rm acc} - \dot{M}_{\rm nuc} = 0$). The decrease in the envelope mass is supplied by the mass accretion. Thus, if we continue the mass accretion, hydrogen-shell burning will never end. If we stop the mass accretion, the envelope mass decreases by nuclear burning and the shell flash eventually ends. If we restart the mass accretion after some time later, we obtain the next shell flash. In this way, we have multicycle shell flashes. Figure 6(c) gives an example of the periodic change of the mass-accretion rate. If we stop/restart the mass accretion in our model calculation, we obtain successive shell flashes.

Figure 6 compares characteristic properties of these three models: the photospheric luminosity $L_{\rm ph}$, photospheric temperature $T_{\rm ph}$, and supersoft X-ray light curve $L_{\rm X}$ (0.3–1.0 keV) calculated from $L_{\rm ph}$ and $T_{\rm ph}$, using a blackbody approximation. The photospheric temperature is shown only in the last cycle to avoid complicating the lines. As the photospheric temperature is always high ($\log T_{\rm ph}$ (K) > 5.4), most of photons are emitted in the far-UV and supersoft X-ray bands. As expected, they are all periodic SSSs.

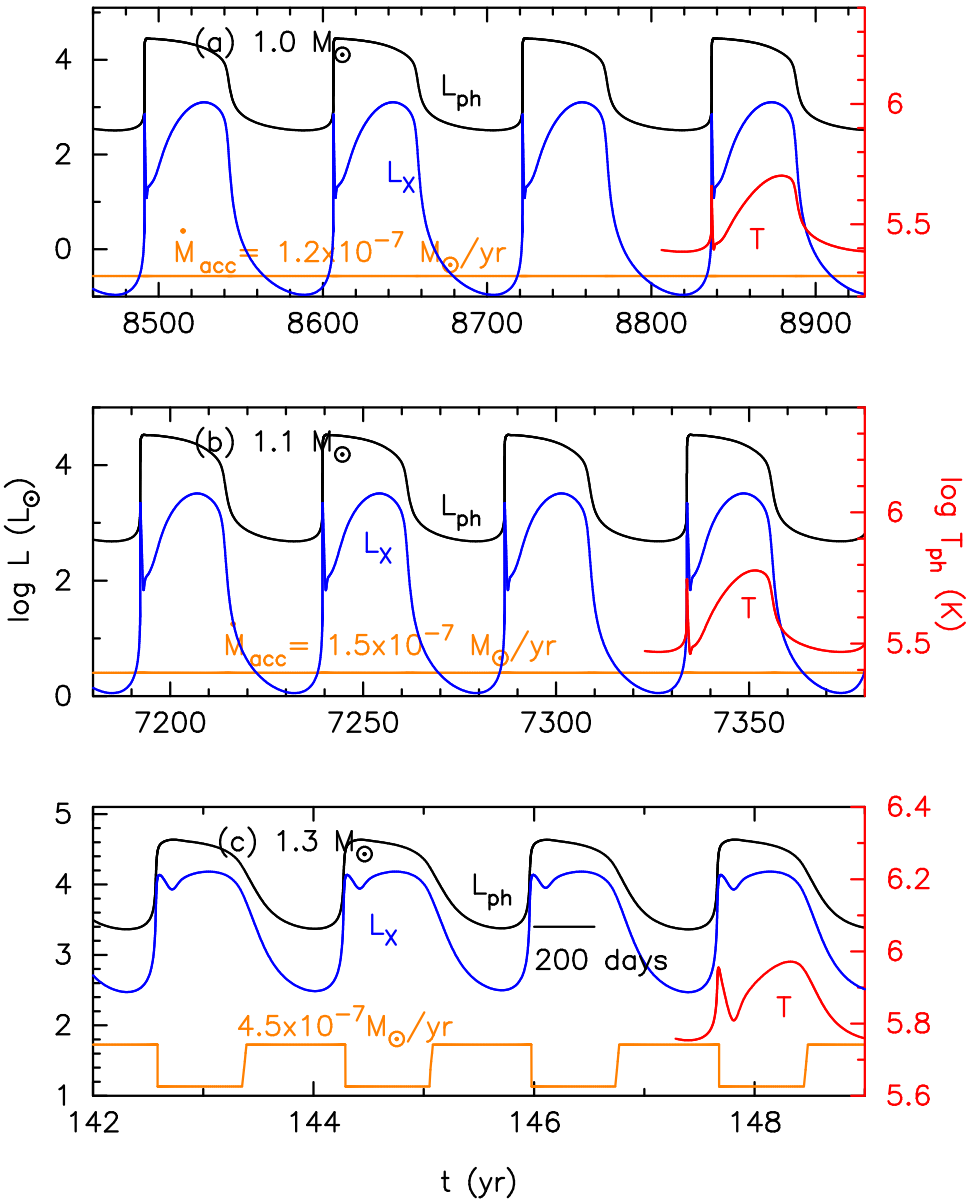

Figure 6. Our models without mass ejection are shown for several flashes: the photospheric luminosity, $L_{\rm ph}$ (black line); supersoft X-ray (0.3–1.0 keV) luminosity, $L_{\rm X}$ (blue line); photospheric temperature, $T_{\rm ph}$ (red line: the last cycle only); and mass-accretion rate, $\dot{M}_{\rm acc}$ (orange line). The chemical composition of accreted matter is assumed to be $X = 0.75$, $Y = 0.249$, and $Z = 0.001$. (a) A 1.0 $M_\odot$ WD with $\dot{M}_{\rm acc} = 1.2 \times 10^{-7}\,M_\odot$ yr^{-1}. (b) A 1.1 $M_\odot$ WD with $\dot{M}_{\rm acc} = 1.5 \times 10^{-7}\,M_\odot$ yr^{-1}. (c) A 1.3 $M_\odot$ WD with $\dot{M}_{\rm acc} = 4.5 \times 10^{-7}\,M_\odot$ yr^{-1}. The models in panels (a) and (b) are natural novae. We do not stop the mass accretion in the outburst phase. The model in panel (c) is a forced nova in which we stop the mass accretion ($\dot{M}_{\rm acc} = 0.0$) and then restart it ($\dot{M}_{\rm acc} = 4.5 \times 10^{-7}\,M_\odot$ yr^{-1}) as denoted by the orange line labeled $4.5 \times 10^{-7}\,M_\odot$ yr^{-1}.

4. Search for Novae Having a Short X-Ray Duration with No Mass Ejection

4.1. Natural Novae

We searched shell-flash models for no mass ejection. Below the stability line, i.e., in the natural novae, we found no-mass-ejection models only in low-mass WDs as shown in Figure 5. In more massive WDs ($M_{\rm WD} \gtrsim 1.1\,M_\odot$), shell flashes are stronger and mass ejection always occurs. The border between with/without mass ejection is about $M_{\rm WD} = 1.0$–$1.1\,M_\odot$ as in Figure 5. This is consistent with the study of the occurrence condition of winds for metal-poor novae (Kato et al. 2013).

Far below the stability line, i.e., with lower mass-accretion rates, the shell flash becomes much stronger, and we have to assume large mass-loss rates during the outburst.

The SSS duration is longer in lower mass WDs. In the 1.0 and 1.1 $M_\odot$ WD models, the massive limit of no-mass-ejection models has the SSS duration much longer than 200 days, which is not consistent with the ASASSN-16oh observation (see Figure 6(c)). Thus, we conclude that there is no natural nova corresponding to ASASSN-16oh.

4.2. Forced Novae

Above the stability line, i.e., in forced novae, the recurrence period can be controlled by manipulating the restarting time of accretion. If we delay the restarting time, the next outburst occurs later even if both the WD mass and mass-accretion rate are the same (Kato et al. 2014; Hachisu et al. 2016). The shell

Table 1
Summary of Forced Nova Models

Model		$M_{\rm WD}$ ($M_\odot$)	Z[a]	$\dot{M}_{\rm acc}$ ($10^{-7}M_\odot$ yr^{-1})	$t_{\rm restart}$[b] (yr)	Mass Loss	$t_{\rm rec}$ (yr)	$L_{\rm nuc}^{\rm max}$ ($10^5L_\odot$)	$M_{\rm acc}$ ($10^{-7}M_\odot$)	η	$\dot{M}_{\rm CO}$ ($10^{-7}M_\odot$ yr^{-1})
A	...	1.32	0.001	5.0	0.55	no	1.1	1.2	2.9	1.0	2.6
B	...	1.32	0.001	5.0	2.6	yes	4.2	10	8.6	0.34	0.64
C	...	1.32	0.001	5.0	5.3	yes	7.3	13	9.5	0.26	0.35
D	...	1.32	0.001	5.2	0.53	no	1.0	1.0	2.7	1.0	2.6
E	...	1.32	0.001	5.2	2.8	yes	4.2	9.5	7.5	0.41	0.72
F	...	1.35	0.0001	5.0	0.58	no	1.1	0.85	2.7	1.0	2.4
G	...	1.35	0.0001	5.0	0.80	no	1.4	1.2	3.3	1.0	2.3
H	...	1.35	0.0001	5.0	1.5	yes	2.5	2.7	5.0	0.75	1.5

Notes.
[a] $X = 0.75$, $Y = 1.0 - X - Z$.
[b] Restarting time of mass accretion since the $L_{\rm nuc}$ peak.

flash becomes stronger because the WD cools down during the delay.

As the recurrence period of forced novae can be controlled, we first search nova sequences for a short X-ray duration regardless of recurrence period. The outburst duration is shorter in more massive WDs. We found that a WD more massive than 1.32 $M_\odot$ can have an X-ray duration shorter than 200 days. In WDs more massive than 1.32 $M_\odot$, however, we have to assume mass loss to continue numerical calculation. Thus, the 1.32 $M_\odot$ WD is the upper mass limit in our calculation that fulfills a short X-ray duration ($\lesssim$200 days) and no mass ejection. In the next subsection, we describe our 1.32 $M_\odot$ WD model in detail.

4.3. 1.32 $M_\odot$ Forced Nova Model

Table 1 summarizes the shell-flash properties of our five 1.32 $M_\odot$ models. It lists the WD mass ($M_{\rm WD}$); metallicity (Z); mass-accretion rate ($\dot{M}_{\rm acc}$); restarting time ($t_{\rm restart}$) of accretion after previous shell flash occurs, i.e., the time from the epoch when the maximum nuclear luminosity is attained; whether or not numerical mass loss is adopted (yes or no); recurrence period ($t_{\rm rec}$); maximum nuclear luminosity ($L_{\rm nuc}^{\rm max}$); amount of accreted matter between two flashes ($M_{\rm acc}$); mass retention efficiency, i.e., the ratio of the mass of ash helium and accreted matter (η); and the mean mass-increase rate of the WD (a CO core with a He layer; $\dot{M}_{\rm CO}$). The properties of Models A and D are almost the same because their mass-accretion rates are not that different. Also, Models B and E are similar. The maximum nuclear luminosity $L_{\rm nuc}^{\rm max}$ represents the flash strength. The flash is stronger for a smaller mass-accretion rate and a later restarting time of accretion.

Figure 7(a) shows two models with no mass ejection, Models A (solid lines) and D (dotted lines). As the mass-accretion rates are almost the same, the light curves are very similar. The next outburst begins a bit later in the smaller mass-accretion model (Model A). The duration of the X-ray light curves are about 200 days in both models.

Figure 7(b) shows Models B, C, and E, models with a later restarting time of mass-accretion. In these cases, the X-ray light curve decays faster than the models in panel (a). The recurrence period becomes longer, 4 yr in Models B and E, and 7 yr in Model C. In our calculation code, we cannot continue our calculation in the expanded stage unless we adopt a numerical mass-loss scheme, the rate of which is shown by the red line in the figure. As shown in Models B and C, we need to assume a larger mass-loss rate for a larger restarting time of mass accretion. This does not directly mean that the mass loss actually occurs because we did not adopt an iteration process to include realistic wind solutions as we did in Kato et al. (2017b). Even if real mass loss occurs, the acceleration is very weak in such a low-Z environment, and the wind velocity would be as small as $\sim$100 km s^{-1} (Kato 1999), which is comparable with the FWHM of the He II line in the optical spectra (Maccarone et al. 2019).

The wind durations of Models B, C, and E are 55–58 days as in Figure 7(b). The winds stopped 84–106 days before the optical detection of ASASSN-16oh. The wind velocity is as small as 100 km s^{-1} or smaller, much smaller than the escape velocity. Therefore, the escaping matter would soon fall back to the equatorial plane and stay as circumbinary matter or merge into the accretion disk. We suppose that the escaping matter (wind) from the WD may not contribute to the He II line at the detection of ASASSN-16oh.

Due to numerical difficulties, we did not calculate other models with similar parameters. We think that the 1.32 $M_\odot$ models are close to the one that is consistent with the observation of ASASSN-16oh.

We show the X-ray count rate of ASASSN-16oh in the decay phase of these theoretical light curves. In this fitting, we regarded the hydrogen-shell flash to have started 200 days before the X-ray detection. The WD was always bright in the X-ray band during this 200 days, but unfortunately, we had no chance of detection until a much later phase. We further assume that a massive mass inflow started shortly before the shell flash started. This mass inflow may be associated with a dwarf nova outburst. The dwarf nova outburst developed from inside to outside of the disk, which results in a slow rise of the V/I light curves. The V/I brightnesses could be brighter than normal dwarf nova outbursts because the disk is irradiated by the hot WD. Irrespective of whether a dwarf nova triggered the nova outburst or a nova outburst triggered a dwarf nova outburst, this picture roughly explains the observational properties of ASASSN-16oh discussed in Section 2.

We also calculated a similar model, but for a lower metallicity, i.e., $Z = 0.0001$, $M_{\rm WD} = 1.35\,M_\odot$, and $\dot{M}_{\rm acc} = 5 \times 10^{-7}\,M_\odot$ yr^{-1}, with different restarting times of accretion. These model properties are listed in Table 1. Models F and G show no mass ejection, but Model H accompanies mass loss. They have very similar X-ray light curves to those in Figure 7.

The models except Model C show recurrence periods shorter than 6 yr. This does not match the observation of ASASSN-

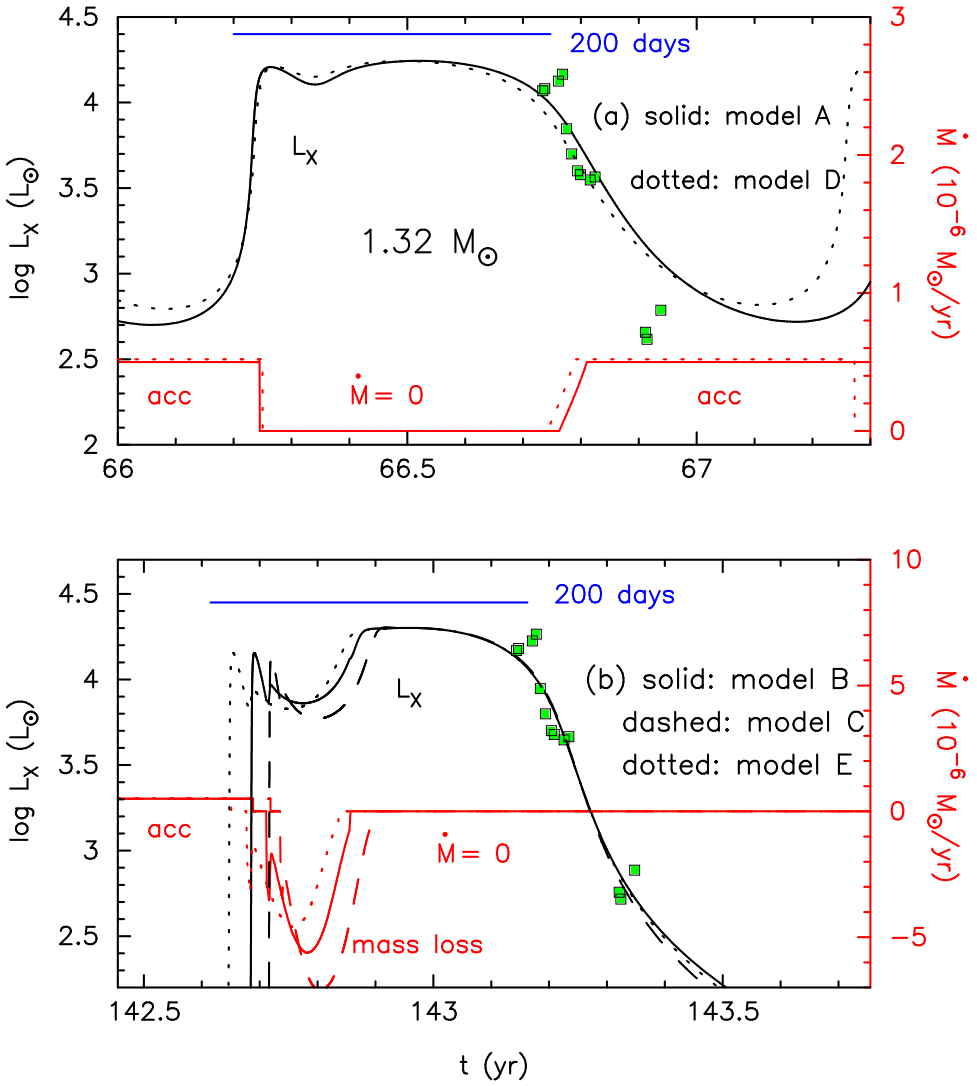

Figure 7. Close-up view of L_X (0.3–1 keV) in our forced nova model of a 1.32 $M_\odot$ WD. We added the *Swift* data for comparison (filled green square outlined by the black line). (a) Model A: $\dot{M}_{acc} = 5 \times 10^{-7}\,M_\odot$ yr^{-1} (solid line) and Model D: $\dot{M}_{acc} = 5.2 \times 10^{-7}\,M_\odot$ yr^{-1} (dotted line). We stop the mass accretion in the bright phase. Wind mass loss does not occur. (b) Same as the models in panel (a), but with a delay of mass accretion. Model B: solid line. Model C: dashed line. Model E: dotted line. The accretion restarts 2.6 yr after the L_{nuc} maximum in Model B, while 5.3 yr in Model C and 2.8 yr in Model E. The assumed mass-loss rates are depicted by the red lines.

16oh, because at least a 6 yr quiescent phase is obvious prior to the outburst from the OGLE IV data (Maccarone et al. 2019).

To summarize, searching for a model having a short X-ray duration (<200 days), no mass- ejection, and long recurrence period (>6 yr), we find that the 1.32 $M_\odot$ WD ($Z = 0.001$) model is the closest one to the ASASSN-16oh observation.

The mass retention efficiency is $\eta = 1.0$ for no-mass-ejection models and $\eta = 0.3$–0.4 for mass-ejection models. After one cycle of hydrogen-shell flash, the ash helium accumulates on the CO core. This mass-increase rate of the CO core is listed in the last column of Table 1, with amounts as large as $\dot{M}_{CO} > 2 \times 10^{-7} M_\odot$ yr^{-1} for no-mass-ejection models.

4.4. Shell Flashes in the Hertzsprung–Russell Diagram

It is instructive to show how shell flashes behave in the Hertzsprung–Russell (HR) diagram. Figure 8 shows shell-flash tracks in the HR diagram for the last cycle of our three models, 1.32 $M_\odot$ WD (black line), 1.1 $M_\odot$ WD (blue line), and 1.0 $M_\odot$ WD (red line). These models are already shown in Figures 7 (Model A), 6(b), and (a), respectively.

As the shell flash proceeds, the WD starts from the bottom of the curve and brightens up and turns to the right in the HR diagram. The maximum expansion of the WD photosphere depends on the ignition mass. In these models, the ignition masses are very small so their envelopes do not extend beyond 0.1 $R_\odot$ (thin black line). This properties are already studied with hydrostatic approximation in Kato & Hachisu (2009) for $Z = 0.02$.

The thin orange line labeled as L_{ph} shows a sequence of hydrostatic solutions that represents a theoretical nova outburst on a 1.1 $M_\odot$ WD with a very large ignition mass of the hydrogen envelope. Here we assume that the chemical composition of the envelope is $X = 0.75$, $Y = 0.249$, and $Z = 0.001$ and the original WD radius underneath the hydrogen-rich envelope is $\log(R_{WD}/R_\odot) = -2.104$ taken from the 1.1 $M_\odot$ model with the mass-accretion rate of $\dot{M}_{acc} = 1.5 \times 10^{-7}\,M_\odot$ yr^{-1}. It should be noted that the photospheric luminosity in the upper branch (horizontal part

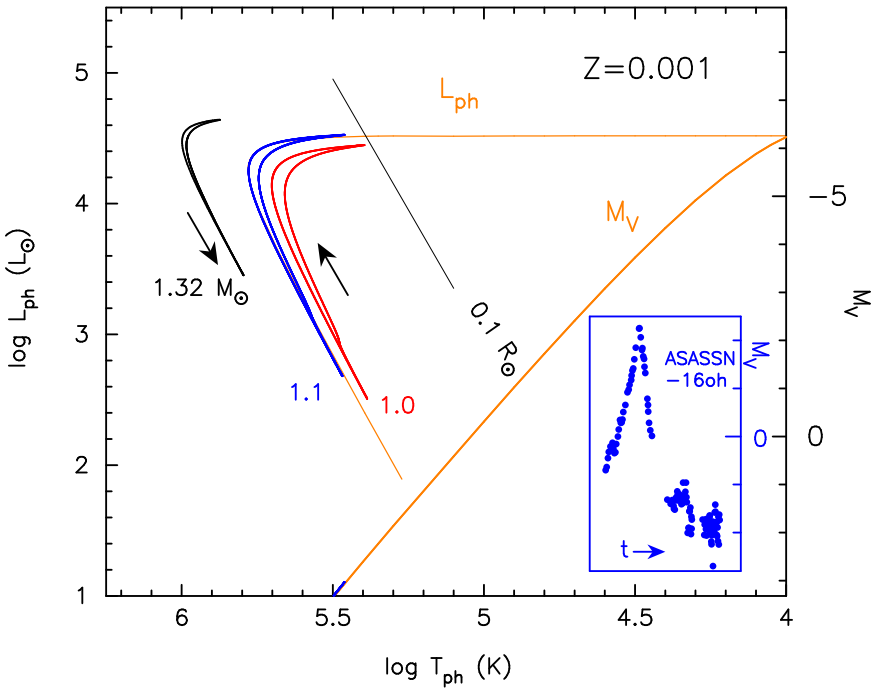

Figure 8. One cycle of shell flashes in the HR diagram. All the models have no mass-ejection. From left to right. Black line: a 1.32 $M_\odot$ WD with $\dot{M}_{\rm acc} = 5 \times 10^{-7}\,M_\odot$ yr^{-1} (Model A in Table 1). Blue line: a 1.1 $M_\odot$ WD with $\dot{M}_{\rm acc} = 1.5 \times 10^{-7}\,M_\odot$ yr^{-1} in Figure 6(b). Red line: a 1.0 $M_\odot$ WD with $\dot{M}_{\rm acc} = 1.2 \times 10^{-7}\,M_\odot$ yr^{-1} in Figure 6(a). The black arrows indicate the direction of evolution. The thin orange line shows the track of the sequence of static solutions that represent a theoretical nova outburst on a 1.1 $M_\odot$ WD with a very large ignition mass. The thick orange line labeled M_V is the absolute V magnitude on the right-side ordinate, calculated from the temperature ($T_{\rm eff}$) and luminosity ($L_{\rm ph}$) of the thin orange model in the upper (bright) branch. We also add the M_V of the upper branch in the 1.1 $M_\odot$ model (blue line model), which appears in the very bottom region on the thick orange line. The thin black line indicates the locus of $R_{\rm ph} = 0.1\,R_\odot$. The inset shows the M_V light curve of ASASSN-16oh, the same data in Figure 1, but shifted by $(m - M)_V = 19.0$. The naked WD without an irradiated accretion disk is darker than $M_V > 3$ and cannot reproduce the V brightness of ASASSN-16oh.

of the thin orange line) is almost the same as the Eddington luminosity.

The thick orange line labeled as M_V denotes the absolute V magnitudes corresponding to the sequence of the thin orange line. Here we have calculated the absolute V magnitude M_V from $T_{\rm ph}$ and $L_{\rm ph}$ with the blackbody approximation. The contributions from the accretion disk and companion star are not included. This figure is similar to Figure 15 of Iben (1982). Even if the $L_{\rm ph}$ is constant, the M_V is smaller (brighter) for a lower $T_{\rm ph}$ because of different bolometric corrections. In our models, the photospheric temperature does not decrease much ($\log T_{\rm ph}$ (K) > 5.4), so the V brightness is rather faint. For example, our 1.1 $M_\odot$ WD model (blue line) reaches the maximum at $M_V = 3$ as shown by the blue part on the lower orange line labeled M_V.

The inset shows the absolute V magnitudes of ASASSN-16oh. Its maximum brightness reaches $M_V \sim -2.3$, which is much brighter than the naked WD. It is obvious that there is another source in the V/I brightnesses of ASASSN-16oh.

5. Comparison with Hillman et al.'s (2019) Calculation

Hillman et al. (2019) presented a nova model with no mass ejection for ASASSN-16oh. This model is based on the idea that both the V/I photons and X-rays are emitted from the hot WD surface. Their best-fit I light curves are obtained for $M_{\rm WD} = 1.1\,M_\odot$ and $\dot{M}_{\rm acc} = (3.5\text{–}5) \times 10^{-7}\ M_\odot$ yr^{-1}.

In Section 4, however, we searched for possible nova models of ASASSN-16oh and obtained the WD mass to be $M_{\rm WD} \gtrsim 1.32\,M_\odot$, much more massive than Hillman et al.'s. As the mass-accretion rate of $\dot{M}_{\rm acc} = 5 \times 10^{-7}\,M_\odot$ yr^{-1} is above the stability line, we need some on/off-switch mechanism of mass accretion, otherwise we have steady-state burning (see Figure 1 of Hachisu et al. 2016). In other words, a forced nova does not occur in nature without some mechanism of an on/off switch. In our model, this on switch is a mass accretion during a dwarf nova outburst. As shown below, Hillman et al.'s model is a forced nova with manipulated mass accretion in their computer code, although no description about this on/off switch is given.

We calculated a shell-flash model with the same parameters as Hillman et al., i.e., $M_{\rm WD} = 1.1\,M_\odot$, $\dot{M}_{\rm acc} = 5 \times 10^{-7}\,M_\odot$ yr^{-1}, and $X = 0.7$, $Y = 0.298$, and $Z = 0.002$. As shown in Figure 9(a), we have successive hydrogen-shell flashes only if we manipulate the mass accretion as indicated by the red line. The photospheric luminosity $L_{\rm ph}$, temperature $T_{\rm ph}$, and supersoft X-ray luminosity $L_{\rm X}$ in the last cycle of our calculation are shown in Figure 9(b). Figure 9(c) shows the V light curve of our model. The M_V magnitudes are calculated from $L_{\rm ph}$ and $T_{\rm ph}$ with the V-band response function and converted to the V magnitudes with the distance modulus of $\mu_V \equiv (m - M)_V = 19.0$ in the V band for ASASSN-16oh.

Figure 9(c) also shows the V-band light curve of ASASSN-16oh (blue dots) in comparison with our WD model. Our model light curve (black line) is much fainter, by 6 mag at the peak, than ASASSN-16oh. The solid red line indicates the V light curve calculated by Hillman et al. (2019, taken from their Figure 2). The peak magnitude is comparable to that of ASASSN-16oh, but decays much slower. The V light curve agrees well with our light curve if we assume $(m - M)_V = 13$ as shown by the dotted red line. We suspect that Hillman et al.

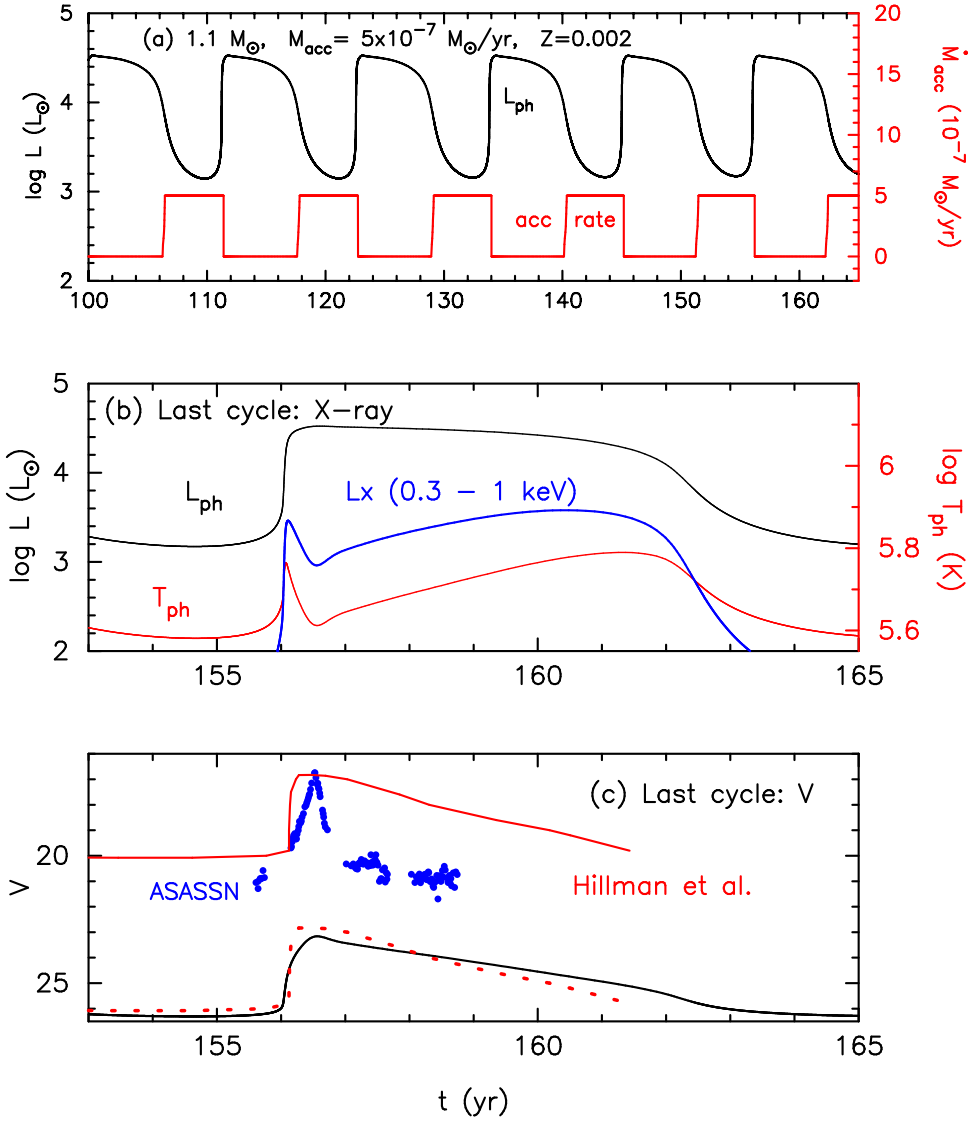

Figure 9. A shell-flash model on a 1.1 $M_\odot$ WD with the mass-accretion rate of $\dot{M}_{\rm acc} = 5 \times 10^{-7}\,M_\odot\,{\rm yr}^{-1}$ for the chemical composition of $X = 0.70$, $Y = 0.298$, and $Z = 0.002$. These parameters are taken from Hillman et al. (2019). (a) The photospheric luminosity (black line) and manipulated mass-accretion rate (red line) that we adopted to mimic Hillman et al.'s model. (b) Close-up view of the last cycle in panel (a). The photospheric luminosity (black line), photospheric temperature (red line), and supersoft X-ray luminosity (0.3–1.0 keV: blue line). (c) The model V light curve (black line) calculated from the luminosity and temperature shown in panel (b). Here, we adopt $\mu_V \equiv (m - M)_V = 19.0$ for ASASSN-16oh. The estimated V-band light curve of ASASSN-16oh (in Figure 1) is added in the same timescale for comparison (blue dots). ASASSN-16oh is much brighter, by ∼6 mag, than our theoretical model. We also add the V light curve (solid red line) of Hillman et al.'s model (taken from Figure 2 of Hillman et al. 2019). This line agrees well with our model V light curve if we shift it down by 6 mag (dotted red line).

might wrongly adopt $(m - M)_V = 13$ (rather than 19) for the distance modulus in V band of ASASSN-16oh.

To summarize, we find that Hillman et al.'s light curve is fainter than that of ASASSN-16oh by 6 mag and decays 10 times slower.

6. Comparison with Maccarone et al.'s Model

Our shell-flash model and Maccarone et al.'s (2019) spreading layer model predict qualitatively similar observational properties. Both models predict supersoft X-rays of blackbody spectrum from optically thick matter on a massive WD. Both models are based on a dwarf nova outburst, in which the accretion disk and companion star are more or less irradiated by X-rays from the WD.

The main difference is in the emitting area and luminosity of X-ray radiation, corresponding to the different energy sources. In our shell-flash model, nuclear burning is the energy source and the whole WD surface is bright. In the spreading layer model, the gravitational energy is released in the inner edge of the accretion disk, and the X-ray-emitting region is concentrated on the equatorial belt. These differences result in different observational properties, which we discuss in the following subsections.

6.1. Total Flux and Binary Inclination of ASASSN-16oh

In the spreading layer model, the maximum luminosity is roughly estimated from gravitational energy release,

$$L^{\rm acc} = \frac{GM_{\rm WD}\dot{M}_{\rm acc}}{2R_{\rm WD}}. \quad (1)$$

For a $1.3\,M_\odot$ WD with $\dot{M}_{\rm acc} = 3 \times 10^{-7} M_\odot\ {\rm yr}^{-1}$ and $R_{\rm WD} = 3 \times 10^8$ cm, we have $L^{\rm acc} = 5.2 \times 10^{36}\,{\rm erg\ s}^{-1}$. On

the other hand, our 1.32 $M_\odot$ WD model in Figure 7 emits $L_{\rm ph} = 1.2 \times 10^{38}$ erg s^{-1}, 23 times larger than the spreading layer emission.

As introduced in Section 2, Maccarone et al. (2019) estimated the X-ray luminosity from the *Chandra* spectrum of ASASSN-16oh to be 6.7×10^{36} erg s^{-1}. This value is consistent with the gravitational energy release from the spreading layer. Hillman et al. (2019) also obtained the unabsorbed X-ray flux to be (4.3–6.4) $\times 10^{36}$ erg s^{-1}. They adopted a thermonuclear runaway model, which would emit an X-ray luminosity of about 10^{38} erg s^{-1}, so they explained the observed small X-ray flux by occultation of the WD surface as in U Sco. We also assume the occultation of the WD surface by the inflated disk edge, that is, we cannot directly observe the WD emission but detect scattered photons which are much fewer than the original WD emission. It could occur if the binary inclination is high enough like in U Sco.

Maccarone et al. (2019) estimated the inclination angle of the binary from the span of the velocity variation in the He II line (75 km s^{-1}). They assumed that the He II line comes from the central part of the accretion disk. For a binary consisting of a 1.3 $M_\odot$ WD and 0.7 $M_\odot$ companion, they obtained the binary inclination from Keplerian law to be $i = 12°$ for an orbital period of $P_{\rm orb} = 1$ day, and $i = 27°$ for $P_{\rm orb} = 10$ days. This value should be replaced by $i = 23°$ and $i = 59°$, respectively, because the authors misplaced the masses of the WD and donor in their calculation.

The above argument on the inclination angle of the binary should be modified if the He II emission line is associated with the hot spot or irradiated companion. If the emitting region is close to the center of mass of the binary, the small line velocities are obtained even in a high inclination binary. Also the line velocity span may not always represent the radial velocity amplitude because of the sparse observation.

The accretion disk around a very hot WD may not be geometrically thin but could be inflated. The disk surface absorbs part of the supersoft X-ray flux from the WD to become hot and emit higher energy photons. This irradiation and reprocessing make the accretion disk inflated and brighter. Popham & Di Stefano (1996) assumed a $\tan^{-1}(z/\varpi) = 15°$ inflation in the UV–optical spectrum model for CAL 83 and RX J0513.9−6951. Schandl et al. (1997) adopted an inflated disk shape with angle up to $\tan^{-1}(z/\varpi) = 24°$ in the light-curve model of the LMC SSS CAL 87. Hachisu et al. (2000) adopted $\tan^{-1}(z/\varpi) = 17°$ at the edge of the disk in their light-curve model of the U Sco 1999 outburst. Here, z is the height of the disk surface from the equatorial plane and ϖ is the distance from the central WD.

The inclination angle of the binary could be one of the key parameters to distinguish the two models. If ASASSN-16oh is an eclipsing binary, it strongly supports the shell-flash model rather than the spreading layer model. If the binary is face on, the faint X-ray flux of ASASSN-16oh is consistent with the spreading layer model, while the shell-flash model needs some explanation for the faint X-ray flux. The present status indicates that the observational clues are not sufficient to draw a definite conclusion.

6.2. UV/Optical SED

Figure 4 shows the SED of ASASSN-16oh (Maccarone et al. 2019). This spectrum resembles those of RX J0513.9−6951 taken by Pakull et al. (1993) in the optical high state. RX J0513.9−6951 is a binary consisting of a massive WD that undergoes steady hydrogen burning, an irradiated accretion disk, and an irradiated companion. Hachisu & Kato (2003) made light-curve models (solid magenta line in Figure 3(b)) in which the irradiated disk mainly contributes to the optical brightness. The resemblance with RX J0513.9−6951 indicates the presence of a bright irradiated accretion disk and companion in ASASSN-16oh.

Popham & Di Stefano (1996) calculated a composite spectrum for LMC persistent SSSs (thick solid black line in Figure 4). Their model binary consists of a hydrogen-burning WD of 1.2 $M_\odot$, irradiated accretion disk with a radius of 1.9 $R_\odot$, and Roche-lobe-filling 2 $M_\odot$ main-sequence companion. The orbital period is $P_{\rm orb} = 1$ day. The inflated accretion disk ($\tan^{-1}(z/\varpi) = 15°$ at its outer edge) is irradiated and brightened 19 times at $\lambda = 1000$ Å, and 4 times at $\lambda = 6300$ Å. As a result, the total flux, the summation of these three components, reproduces the $F_\lambda \propto \lambda^{-2.33}$ law. The WD does not contribute much in the UV/optical region, but the hydrogen-burning WD is necessarily because its large luminosity is the source of irradiation.

The composite spectrum by Popham and Di Stefano is fainter by $\Delta \log F_\lambda \sim 0.3$ than that of observed ASASSN-16oh data. They assumed the WD luminosity of $L_{\rm WD} = 1.5 \times 10^{38}$ erg s^{-1}, which is comparable to our H-burning WD model (1.2×10^{38} erg s^{-1}). If we assume that ASASSN-16oh is a binary of a 1.3 $M_\odot$ WD and a 0.7 $M_\odot$ companion with $P_{\rm orb} = 5$ days, the binary separation a is $((1.3 + 0.7)/(1.2 + 2))^{1/3}\ 5^{2/3} = 2.5$ times larger than Popham and Di Stefano's model. If we scale up the binary size by a factor of 2.5, without changing the configuration, the irradiated area of the disk and companion become $2.5^2 = 6.25$ times larger. This makes the flux increase by $\Delta \log F_\lambda \sim \log 6.25 = +0.80$. If we adopt the binary inclination of 80°, instead of Popham and Di Stefano's 60°, then, the flux decrease owing to inclination is calculated to be $\log(\cos 80°/\cos 60°) = -0.46$. Then, the flux calculated by Popham and Di Stefano should be increased by 0.80–0.46 = 0.34 for our assumed binary. The resultant spectral energy distribution is very consistent with that of ASASSN-16oh obtained by Maccarone et al. (2019).

In the spreading layer model, the irradiation effect is small because the X-ray luminosity is small. The main contributor in the UV/optical range is the dwarf nova outburst. In general, the absolute flux of a dwarf nova is smaller than those shown in Figure 4 and the wavelength dependence was reported to be $F_\lambda \propto \lambda^{-\Gamma}$, $\Gamma \sim 1.5$–2.3 in the UV/optical range (e.g., Parikh et al. 2019).

6.3. X-Ray Light Curve

In our shell-flash model, the X-ray flux begins to decrease when hydrogen burning almost dies out and the burning zone temperature gradually decreases. The speed of cooling depends on the WD mass; a more massive WD cools faster.

Figure 3(a) compares the light curves of ASASSN-16oh with those of U Sco in a normalized timescale. U Sco hosts a massive WD, 1.37 $M_\odot$ (Hachisu et al. 2000), more massive than our 1.32 $M_\odot$ for ASASSN-16oh, and then the cooling time is much shorter.

When the X-ray flux decreases with time, the irradiation effects decrease so that the UV/optical fluxes from the irradiated disk and companion also become faint. Thus, both

the X-ray and optical fluxes decrease at the same time. In this way, our shell-flash model naturally explains the simultaneous behavior in the X-ray and optical fluxes along with those of U Sco as in Figure 3(a).

In the spreading layer model, the optical flux decreases when the dwarf nova outburst approaches its end. As the X-ray flux is closely related to the mass-accretion rate onto the WD, the expected X-ray count rate decreases with a decrease in the optical flux (e.g., Osaki 1996). It is, however, unknown whether a dwarf nova outburst could show a simultaneous decrease, like in U Sco, in both the X-ray and optical fluxes in the normalized timescale in Figure 3(a).

6.4. Nondetection of Supersoft X-Rays in the Quiescent Phase of RS Oph

RS Oph is a recurrent nova that hosts a massive WD with high mass-accretion rate ($1.35\,M_\odot$ and $1.2\times10^{-7}\,M_\odot$ yr^{-1}: Hachisu & Kato 2001; Hachisu et al. 2006). The WD mass and mass-accretion rate are more or less similar to those of ASASSN-16oh. If the X-ray emission of ASASSN-16oh is emitted from the optically thick spreading layer, we may expect supersoft X-rays in the quiescent phase of RS Oph.

Nelson et al. (2011) observed quiescent phase of RS Oph with the *Chandra* and *XMM-Newton* satellites, 537 and 744 days after the nova outburst. They analyzed the spectrum and obtained the maximum allowable blackbody temperature for an optically thick component of the spreading layer to be 0.034 keV ($=3.9\times10^5$ K). The upper limit of unabsorbed luminosity is $(1.1\text{–}1.6)\times10^{35}(d/1.6\ \mathrm{kpc})^2$ erg s^{-1}, where d is the distance to the star. This upper limit is smaller than those detected in ASASSN-16oh by a factor of 40.

The boundary layer between a WD and the inner edge of the accretion disk has been studied by various authors. (Popham & Narayan 1995; Piro & Bildsten 2004, and references therein.) If the mass-accretion rate is large, the boundary layer is geometrically thin, optically thick, and emits supersoft X-rays. When the accretion rate decreases, the boundary layer becomes optically thin, geometrically thick, and emits hard X-rays.

Popham & Narayan (1995) calculated the mass-accretion rate at this transition. For a $1.0\,M_\odot$ WD, the critical mass-accretion rate is $\log \dot{M}_{\rm acc}\ (M_\odot\ \mathrm{yr}^{-1}) = -6.12$. This value depends on the model parameters, e.g., such as the WD rotation rate and viscosity parameter. They did not calculate for $M_{\rm WD} > 1.0\,M_\odot$, but from the tendency for a quick increase with the WD mass, the transition may occur at $\log \dot{M}\ (M_\odot\ \mathrm{yr}^{-1}) \sim -5$ for $1.3\,M_\odot$. Below this rate, the boundary layer is optically thin and would emit hard X-rays. A small accretion rate may be the reason why the supersoft X-ray component was not detected in the quiescent phase of RS Oph.

If the same argument is applied to ASASSN-16oh with an accretion rate of $3\times10^{-7}\,M_\odot$ yr^{-1}, the boundary layer should be optically thin and a hard X-ray component has to be expected during the outburst. However, there are no hard X-ray components in the spectrum (Maccarone et al. 2019). The possible reasons for the absence of hard X-rays are:

(1) A hot optically thin extended boundary layer was formed and emitted hard X-rays. However, the X-rays were occulted by the inflated disk edge and undetected, or its flux was too small to be detected.
(2) The mass accretion had already stopped before the period of observation.

6.5. Summary

The resemblance of the $V-I$ color (Figure 2) and absolute magnitude M_V (Figure 3) indicates that ASASSN-16oh is a binary system consisting of a hydrogen-burning WD, irradiated accretion disk, and lobe-filling companion star. The spectral energy distribution $F_\lambda \propto \lambda^{-2.33}$ (Figure 4) can be explained by the sum of contributions from an accretion disk and a companion star, which are irradiated by a WD in the luminous stage of a shell flash. Our shell-flash model is consistent with these three properties. We further show that the simultaneous declines in the X-ray and optical are also explained by our hydrogen-burning model (Section 6.3) and that our hydrogen-burning model is consistent with undetected hard X-ray flux even for the optically thin boundary layer case (Section 6.4).

ASASSN-16oh is an atypical dwarf nova in its slow rise/decay and large amplitude. It is very helpful to see if similarly shaped dwarf novae show similar color and brightness to ASASSN-16oh.

7. Discussion

7.1. A Dwarf Nova Triggers a Nova Outburst?

We examine the possibility of a dwarf nova outburst triggering a nova outburst.

An accreting WD will experience a nova outburst when the mass of the hydrogen-rich envelope reaches a critical value. Table 1 lists the amount of accreted matter to trigger hydrogen ignition. They are a few to several times $10^{-7}\,M_\odot$. This ignition mass is smaller for a shorter recurrence period because the WD surface is hotter.

On the other hand, the mass-inflow rate onto the WD is estimated in several dwarf novae (Kimura et al. 2018). Among them, V364 Lib shows a relatively large mass-inflow rate of $1\times10^{-7}\,M_\odot$ yr^{-1} (Kimura et al. 2018). This object has an orbital period of $P_{\rm orb} = 0.70$ days, rising (decay) time of 10 (35) days, and small outburst amplitude of 1 mag. As ASASSN-16oh has a much larger outburst amplitude and longer orbital period, we may expect a larger mass-inflow rate. If we assume the mass-inflow rate of several times $10^{-7}\,M_\odot$ yr^{-1}, the WD may accrete sufficient mass for hydrogen ignition. Our calculation assumed a periodic change of mass accretion, but in the real world, the mass inflow may occur irregularly. If WDs accrete sufficient mass through one or several times of mass-accretion events with a large mass-inflow rate, a weak shell flash may occur similarly to ASASSN-16oh.

7.2. Forced Novae

Nova outbursts with high mass-accretion rates have been calculated by many authors (Prialnik & Kovetz 1995; Yaron et al. 2005; Idan et al. 2013; Hillman et al. 2015, 2019). Forced nova phenomena are studied in detail by Kato et al. (2014) and by Hachisu et al. (2016) in which they pointed out that forced novae are already calculated without recognizing it because they automatically switched on/off the mass accretion in their numerical codes. In the cases with very high mass-accretion rates, characteristic properties are similar to those in Figure 6, i.e., no mass ejection and a short quiescent phase comparable to the shell-flash duration.

The forced novae are still theoretical objects because no mechanism of switching on/off is identified. If the ASASSN-

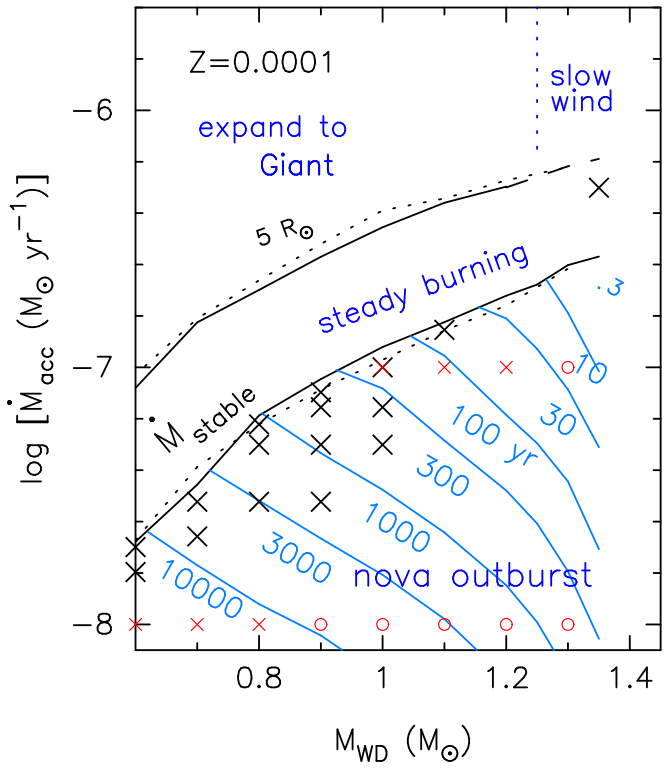

Figure 10. Same as Figure 5, but for Z = 0.0001. The small red crosses, open red circles, and two dotted black lines are taken from Chen et al. (2019). See the main text for more details.

16oh outburst is a shell-flash phenomenon triggered by a dwarf nova, this is the first observational support for a forced nova.

In the forced novae, the mass-accretion rate is very high by its definition, so the shell flash could be weak. Thus, the mass retention efficiency of the WD is very high. Especially with no mass ejection, the mass retention efficiency of the WD is ∼100%. Such an object is a candidate of SN Ia progenitors. In this sense, ASASSN-16oh is a promising object.

7.3. Novae in a Very Low Metallicity of Z = 0.0001

Nova outbursts in various metallicities were systematically studied by Kato (1997, 1999) and by Kato et al. (2013). The optically thick winds, the main mechanism of mass loss during the nova outbursts, are accelerated owing to the prominent iron peak in the radiative opacity at $\log T$ (K) ∼ 5.2. For a lower metallicity, this Fe peak is small and almost disappears in $Z \lesssim 0.0004$. In such a case, another peak due to He ionization ($\log T$ (K) ∼ 4.7, see Figure 4 of Kato et al. 2013 for opacities) works as the driving source.

Kato et al. (2013) showed that the Fe opacity peak works to drive the winds for a wide range of WD masses ($M_{\rm WD} > 0.5\,M_\odot$) for $Z = 0.02$. For $Z = 0.001$, it works only in massive WDs ($M_{\rm WD} > 1.05\,M_\odot$) and the main driving source is replaced by the He opacity peak in less massive WDs. For $Z \leqslant 0.0004$, only the He opacity peak works because the Fe peak disappears. The acceleration by the He opacity peak may be weak because its peak is small. Thus, we expect weak mass ejection or slow expansion. Observational counterparts of such phenomena are not identified yet, and then, it is not known if such a weak wind results in a nova outburst with efficient mass ejection from the binary.

Figure 10 shows the stability line and recurrence periods for the composition of $X = 0.75$ and $Z = 0.0001$. In the same figure, we added the results by Chen et al. (2019). The small red crosses denote flashes with no mass ejection, and the small open red circles are for those with mass loss. Their results are consistent with ours.

This plot also shows their stability line (lower dotted line) and their expansion line above which the WD envelope increases (upper dotted line). These two lines are consistent with our $\dot{M}_{\rm stable}$ and $5\,R_\odot$ lines.

7.4. Metallicity Dependence of the Stability Line

The stability line has been calculated by many authors (Nomoto et al. 2007; Ma et al. 2013; Wolf et al. 2013a, 2013b; Kato et al. 2014, for $Z = 0.02$), (and Chen et al. 2019, for $Z = 0.0001$). Our stability lines are lower than those of $X = 0.7$ and $Z = 0.02$ (Kato et al. 2014) by a factor of 0.8–0.9 (vertically lower by 0.05–0.1 dex) for $X = 0.75$ and $Z = 0.001$ in Figure 5, and by a factor of 0.6–0.8 (vertically lower by 0.1–0.2 dex) for $X = 0.75$ and $Z = 0.0001$ in Figure 10.

The stability line shows the minimum mass-accretion rate below which the hydrostatic envelope cannot keep the temperature high enough to support steady nuclear burning (point B in Figure 1 of Kato et al. 2014). For the same WD mass and accretion rate, the envelope mass is larger for a lower Z because of a difference in the opacity. Thus, the temperature at the bottom of the envelope is also high. This makes a difference in the stability line.

7.5. Metallicity Dependence of the Recurrence Period

Figure 5 also shows the equi-recurrence period line. The recurrence period is shorter for massive WDs and higher mass-accretion rates.

The equi-recurrence period lines were obtained for the solar composition ($X = 0.7$ and $Z = 0.02$) by Kato et al. (2014) and by Hachisu et al. (2016). Our equi-recurrence period lines are systematically longer than their equi-period lines by a factor of ∼1.4 (shifted by 0.15 dex upward) in Figure 5 (for $X = 0.75$ and $Z = 0.001$) and by a factor of ∼1.8 (shifted by 0.25 dex upward) in Figure 10 (for $X = 0.75$ and $Z = 0.0001$).

For a lower Z, the ignition mass is larger because the lower opacity results in a lower blanket effect, and it takes more time until a hydrogen ignition occurs at the bottom of the accreted matter. Thus, for the same WD mass and mass-accretion rate, it takes a longer accretion time until the flash begins.

8. Conclusions

Our main results are summarized as follows.

1. We summarize the observational properties of ASASSN-16oh from the view point of an irradiated accretion disk model. The X-ray count rates are consistent with the scattered flux from the obscured WD in the SSS phase of the recurrent nova U Sco. The $V - I$ color, peak M_V, and $F_\lambda \propto \lambda^{-2.33}$ law are quite consistent with the large irradiated accretion disks of U Sco and RX J0513.9 −6951. Thus, we may conclude that the supersoft X-ray fluxes originate from the hydrogen-burning WD, while the V- and I-band fluxes come from the irradiated accretion disk.

2. Supposing that a dwarf nova triggers a forced nova, we are able to obtain the X-ray light curve consistent with ASASSN-16oh, i.e., a short X-ray duration (<200 days) and no mass ejection. We found a $1.32\,M_{\odot}$ WD model is the closest one for the low-metallicity environment of $Z = 0.001$. If it is the case that ASASSN-16oh is a dwarf nova and it triggers a nova, this is the first identified forced nova that occurs above the stability line.
3. We have calculated a shell-flash model with the same parameters as those in Hillman et al. (2019) and found that their models are forced novae in which the mass-accretion on/off switch was manipulated in the computer code. We have found that their light curve to fit with ASASSN-16oh is based on too small a distance modulus for the SMC; when corrected, the peak and decay timescales are very different from those of ASASSN-16oh.
4. The galactic nova PU Vul was first observationally identified as a no-mass-ejection nova, but it occurred on a low-mass WD ($\sim 0.6\,M_{\odot}$). If ASASSN-16oh is a thermonuclear runaway object like PU Vul, it will be the second identified no-mass-ejection nova. No-mass-ejection novae hosting a very massive WD are a new type of SSSs in low-Z environments. They could be candidate SN Ia progenitors because the mass retention efficiency is very high ($\eta \sim 100\%$).

We thank the anonymous referee for useful comments that improved the manuscript.

ORCID iDs

Mariko Kato https://orcid.org/0000-0002-8522-8033
Izumi Hachisu https://orcid.org/0000-0002-0884-7404

References

Bohlin, R. C., Savage, B. D., & Drake, J. F. 1978, ApJ, 224, 132
Chen, H., Woods, T. E., Yungelson, L. R., et al. 2019, MNRAS, 490, 1678
Cioni, M.-R. L. 2009, A&A, 506, 1137
Darnley, M. J., Henze, M., Steele, I. A., et al. 2015, A&A, 580, A45
Evans, P. A., Beardmore, A. P, Page, K. L., et al. 2009, MNRAS, 397, 1177
Güver, T., & Özel, F. 2009, MNRAS, 400, 2050
Hachisu, I., & Kato, M. 2001, ApJ, 558, 323
Hachisu, I., & Kato, M. 2003, ApJ, 590, 445
Hachisu, I., & Kato, M. 2006, ApJS, 167, 59
Hachisu, I., & Kato, M. 2015, ApJ, 798, 76
Hachisu, I., & Kato, M. 2018, ApJS, 237, 4
Hachisu, I., & Kato, M. 2019a, ApJS, 241, 4
Hachisu, I., & Kato, M. 2019b, ApJS, 242, 18
Hachisu, I., Kato, M., Kato, T., & Matsumoto, K. 2000, ApJL, 528, L97
Hachisu, I., Kato, M., Kiyota, S., et al. 2006, ApJL, 651, L141
Hachisu, I., Kato, M., & Luna, G. J. M. 2008, ApJL, 659, L153
Hachisu, I., Saio, H., & Kato, M. 2016, ApJ, 824, 22
Henze, M., Darnley, M. J., Williams, S. C., et al. 2018, ApJ, 857, 68
Hillman, Y., Orio, M., Prialnik, D., et al. 2019, ApJL, 879, L5
Hillman, Y., Prialnik, D., Kovetz, A., & Shara, M. M. 2015, MNRAS, 446, 1924
Iben, I., Jr. 1982, ApJ, 259, 244
Idan, I., Shaviv, N. J., & Shaviv, G. 2013, MNRAS, 433, 2884
Iglesias, C. A., & Rogers, F. J. 1996, ApJ, 464, 943
Imara, N., & Blitz, L. 2007, ApJ, 662, 969
Jha, S. W., Colmenero, E. R., Stanek, K. Z., et al. 2016, ATel, 9859, 1
Kato, M. 1985, PASJ, 37, 19
Kato, M. 1997, ApJS, 113, 121
Kato, M. 1999, PASJ, 51, 525
Kato, M., & Hachisu, I. 1994, ApJ, 437, 802
Kato, M., & Hachisu, I. 2009, ApJ, 699, 1293
Kato, M., Hachisu, I., Cassatella, A., & González-Riestra, R. 2011, ApJ, 727, 72
Kato, M., Hachisu, I., & Henze, M. 2013, ApJ, 779, 19
Kato, M., Hachisu, I., & Saio, H. 2017a, in Proc. Palermo Workshop 2017 on "The Golden Age of Cataclysmic Variables and Related Objects—IV" 315, ed. F. Giovannelli et al. (Trieste: SISSA PoS), 56
Kato, M., Mikołajewska, J., & Hachisu, I. 2012, ApJ, 750, 5
Kato, M., Saio, H., & Hachisu, I. 2017b, ApJ, 838, 153
Kato, M., Saio, H., Hachisu, I., & Nomoto, K. 2014, ApJ, 793, 136
Kimura, M., Kato, T., Maehara, H., et al. 2018, PASJ, 709, 78
Liszt, H. S. 2014, ApJ, 780, 10
Ma, X., Chen, X., Chen, H.-L., Denissenkov, P. A., & Han, Z. 2013, ApJL, 778, L32
Maccarone, T. J., Nelson, T. J., Brown, P. J., et al. 2019, NatAs, 3, 173
Mroz, P., Udalski, A., Wyrzykowski, L., Kozlowski, S., & Poleski, R. 2016, ATel, 9867, 1
Nelson, T., Mukai, K., Orio, M., Luna, G. J. M., & Sokoloski, J. L. 2011, ApJ, 737, 7
Nomoto, K., Saio, H., Kato, M., & Hachisu, I. 2007, ApJ, 663, 1269
Orio, M., Behar, E., Gallagher, J., et al. 2013, MNRAS, 429, 1342
Osaki, Y. 1996, PASP, 108, 39
Pagnotta, A., Schaefer, B. E., Clem, J. L., et al. 2015, ApJ, 811, 32
Pakull, M. W., Moch, C., Bianchi, L., et al. 1993, A&A, 278, L39
Parikh, A. S., Hernández Santisteban, J. V., Wijnands, R., & Page, D. 2019, RMxAA, 55, 55
Pietrzyński, G., Graczyk, D., Gieren, W., et al. 2011, Natur, 495, 76
Piro, A. L., & Bildsten, L. 2004, ApJ, 610, 979
Popham, R., & Di Stefano, R. 1996, in Lecture Notes in Physics, 472 ed. J. Greiner (Berlin: Springer), 66
Popham, R., & Narayan, R. 1995, ApJ, 442, 337
Prialnik, D., & Kovetz, A. 1995, ApJ, 445, 789
Raj, A., Ashok, N. M., Banerjee, D. P. K., et al. 2012, MNRAS, 425, 2576
Rieke, G. H., & Lebofsky, M. J. 1985, ApJ, 288, 618
Salazar, I. V., LeBleu, A., Schaefer, B. E., Landolt, A. U., & Dvorak, S. 2017, MNRAS, 469, 4116
Schaefer, B. E. 2018, MNRAS, 481, 3033
Schaefer, B. E., & Ringwald, F. A. 1995, ApJL, 447, L45
Schandl, S., Meyer-Hofmeister, E., & Meyer, F. 1997, A&A, 318, 73
Schwarz, G. J., Ness, J.-U., Osborne, J. P., et al. 2011, ApJS, 197, 31
Udalski, A., Szymański, M. K., & Szymański, G. 2015, AcA, 65, 1
Walter, F. M., Battisti, A., Towers, S. E., Bond, H. E., & Stringfellow, G. S. 2012, PASP, 124, 1057
Warner, B. 1995, Cataclysmic Variable Stars (Cambridge: Cambridge Univ. Press)
Wolf, W. M., Bildsten, L., Brooks, J., & Paxton, B. 2013a, ApJ, 777, 136
Wolf, W. M., Bildsten, L., Brooks, J., & Paxton, B. 2013b, ApJ, 782, 117, (Erratum)
Yaron, O., Prialnik, D., Shara, M. M., & Kovetz, A. 2005, ApJ, 623, 398